Reply to reviewers' comments on *"Core and margin in warm convective clouds. Part I: core types and evolution during a cloud's lifetime"*

We would like to thank the reviewers for their insightful and helpful comments that help up improve and clarify the manuscript. Before answering all the reviewers' comments in details, we summarize shortly the main modifications done in the manuscript for addressing the main comments:

1. Focused emphasis is now put on the novel parts of this study: the differences between the three core types, their evolutions in time, and comparison to current understanding of core size and location within a cloud.
2. The goals of the work are stated more clearly, and the importance of bin-microphysics is discussed.
3. The introduction was revised significantly to include a more comprehensive review of relevant previous works and the physical processes associated with differences between the core types.
4. The theoretical section is presented as a summary of previous knowledge, with purpose to gain intuitive understanding of the differences between the core types.
5. One cloud field case study was replaced. The revised version presents a continental shallow cumulus convection case study, based on long term observations taken at the ARM Southern Great Plains site.

Please find below a point-by-point reply to all of the reviewers' comments.

Reply to reviewer #1 – RC1

General Reviewer Comment:

This article provides an analysis of the structure of cumulus clouds and the connection between different regions in cumulus clouds. It defines three different regions in the cloud: 1) a Relative Humidity core, where the air is fully saturated, 2) A buoyancy core, here the air is positively buoyant and 3) a vertical velocity core, defined by upwards motion. The authors argue that typically the buoyancy core is a subset of the relative humidity core, which again is a subset of, or at least smaller than, the vertical velocity core. They also consider the effect of mixing on buoyancy and the existence of overshoots as an explanation for this result. I have three key concerns about the draft as it stands, which I think would need to be addressed before publication. More detail on each of these points can be found further below.

1) The main conclusions are not sufficiently novel.

2) There has been significant work on mixing in cumulus clouds in general and on the role of processes at the cloud edge in particular that the current study does not refer to.

3) I have some major concerns about the analysis framework.

Despite the fact that I am critical of the theory and analysis as it stands, I think there is value in analysing the simulations presented here in detail, particularly because many previous studies that have worked on this topic have used an approach to condensation based on immediate saturation adjustment in each grid cell. The use of a spectral bin microphysics model in the context of this a study is therefore valuable, although the difference between the two approaches is not made clear to a sufficient degree. I also realise that there is a follow-up article which may include novel results that might be partially supported by the present work.

I would encourage the authors to either fully revise the study, or to incorporate the parts of the study that are needed to support part II into that article, but still make major changes to these sections to address the concerns below. If the material is not incorporated into part II, it would require a more significant overhaul of the draft than would usually be considered a major revision. However, many previous studies have looked into mixing in cumulus in further detail using SAM, so the authors should be well-placed to improve their analysis. The draft is also generally well-written, so some of the material could likely be reused.

General Answer: We thank the reviewer for the beneficial comments. We revised the paper to be clearer and more complete according to the concerns raised in the review. Please see all the details in the answers below.

Main Comments:

MC1) The conclusions are not sufficiently novel. The two main conclusions are not really new results.

- The role of mixing in rapidly reducing cloud buoyancy has been established in previous theoretical work: e.g. Morrisson (2017) looks into this in detail. This role of mixing in rapidly reducing buoyancy is incorporated in at least three existing parametrisations of cumulus convection (see Kain and Fritsch, 1990; De Rooy and Siebesma, 2008 and Derbyshire et al., 2011). Moreover, the framework of critical mixing fraction used in the studies of Kain and Fritsch and De Rooy and Siebesma already provides a framework for understanding how mixing impacts on buoyancy, and the result that mixing generally reduces buoyancy is well established. There are also a number of existing diagrams that have been used to understand the thermodynamic properties of cumulus clouds, which have also shown mixing generally leads to a region of negative buoyancy (Paluch, 1979; De Roode, 2007). The fact that mixing between core and margin parcels leads to intermediate buoyancy in a near-linear way can also be deduced from previous work (e.g. Pauluis and Schumacher, 2010).

- Similarly, literature on the existence of convective overshoots dates back as far as at least Betts (1973). In order for additional theory to be valuable, it should therefore include predictions that can be directly and quantitatively compared against Large-Eddy Simulation.

MA1) Thank you for this comment. We have revised the manuscript significantly so that clear emphasis is put now on the novel parts of this work: the differences between the three core types, their evolutions in time, and comparison to current understanding of core size and location within a cloud. We are not aware of previous work which tried to perform such a comprehensive analysis and comparison between the different cores. In addition, we describe better in the revised version the previous relevant studies which have dealt with positive vertical velocity and buoyancy in clouds and the effects of entrainment on them.

The new abstract now focuses on the novel aspects of the work:

"The properties of a warm convective cloud are determined by the competition between the growth and dissipation processes occurring within it. One way to observe

and follow this competition is by partitioning the cloud to core and margin regions. Here we look at three core definitions: positive vertical velocity (W_{core}), supersaturation (RH_{core}), and positive buoyancy (B_{core}), and follow their evolution throughout the lifetime of warm convective clouds.

Using single cloud and cloud field simulations with bin-microphysics schemes, we show that the different core types tend to be subsets of one another in the following order: $B_{core} \subseteq RH_{core} \subseteq W_{core}$. This property is seen for several different thermodynamic profile initializations, and is generally maintained during the growing and mature stages of a cloud's lifetime. This finding is in line with previous works and theoretical predictions showing that cumulus clouds may be dominated by negative buoyancy at certain stages of their lifetime.

During its mature growth stage, the cloud and its cores are centered at a similar location. During cloud dissipation the cores show less overlap, typically reduce in size, and migrate from the cloud centroid. In some cases, buoyancy cores can reemerge and often reside at the cloud periphery. Thus, the core-shell model of a positively buoyant center surrounded by negatively buoyant shell only applies to a fraction of the cloud lifetime.”

We see merit in including the rather simple theoretical derivations in the text for the sake of completeness and ease of understanding for a reader who is not an expert in this specific field. We have revised the theoretical section so that it better reflects previous works (see the details in the next answer), but please note that none of those works focused on the relative sizes of the different cores.

MC2) Lack of connection to the existing literature. I am citing a few key studies below but this is by no means a comprehensive list.

- Over the past two decades there has been a large number of studies on the role of negative buoyancy at the cloud edge (e.g., Zhao and Austin 2005; Jonker et al. 2008; Heus and Jonker, 2008), as well as on the implications of the cloud edge for determining effective mixing between clouds and their environment (e.g. Dawe and Austin 2011).

- Similarly, several studies have looked into the role of convective cores in simulations with cloud tracking (e.g. Dawe and Austin 2012, Heus and Seifert 2013), and used this to study the role of these cores throughout the life cycle of the cloud.

MA2) We thank the reviewer for including such an extensive list of relevant previous literature that was indeed lacking in the original manuscript. We have included most of these references (and others) in the revised manuscript, and now try to connect out findings to previous literature wherever found to be of relevance. A few examples are given here, from the introduction:

"***The common assumption when partitioning a convective cloud to its physical core and margin is that that the cloud core is at its geometrical center and the peripheral regions (i.e. edges) are the margin. Previous observational (Heus et al., 2009a; Rodts et al., 2003; Wang et al., 2009) and numerical (Heus and Jonker, 2008; Jonker et al., 2008; Seigel, 2014) works have studied the gradients of cloud thermodynamic properties from cloud center to edge, and suggest that a cloud is best described by a core-shell model. This model assumes a core with positive vertical velocity and buoyancy, surrounded by a shell with negative vertical velocity and buoyancy. The shell is the region where mixing between cloudy and environmental air parcels occurs, leading to evaporative cooling → decrease in buoyancy → decrease in vertical velocity."***

Another part of the introduction:

"Based on previous findings, here we explore the partition of clouds to core and margin using three different objective core definitions where the cloud core threshold is set to be a positive value (of buoyancy, vertical velocity, or supersaturation). Cloud buoyancy (B) can be approximated by the following formula:

$$B = g \cdot \left(\frac{\theta'}{\theta_o} + 0.61q'_v - q_l\right) \qquad (1),$$

Where θ_o represents the reference state potential temperature, q_v is the water vapor mixing ratio, and q_l is the liquid water content. The (') stands for the deviation from the reference state per height (Wang et al., 2009). Buoyancy is a measure for the vertical acceleration and its integral is the convective potential energy. Latent heat release during moist adiabatic ascent fuels positive buoyancy and clouds' growth,

while evaporation and subsequent cooling drives cloud decay (de Roode, 2008; Betts, 1973). The prevalence of negatively buoyancy parcels at the cloud edges due to mixing and evaporation is a well-known phenomenon (Morrison, 2017). Mixing diagrams have been used to assess this effect (de Roode, 2008; Paluch, 1979; Taylor and Baker, 1991), and are at the root of convective parameterization schemes (Emanuel, 1991; Gregory and Rowntree, 1990; Kain and Fritsch, 1990) and parameterizations of entrainment and detrainment in cumulus clouds (de Rooy and Siebesma, 2008; Derbyshire et al., 2011). "

And theoretical section:

"***Hence, for the adiabatic column case,*** $\boldsymbol{B_{core}}$ ***is always a proper subset of*** $\boldsymbol{W_{core}}$ $(\boldsymbol{B_{core} \subset W_{core}})$***. These effects are commonly seen in warm convective cloud fields where permanent vertical layers of negative buoyancy (but with updrafts) within clouds typically exist at the bottom and top regions of the cloudy layer (de Roode and Bretherton, 2003; Betts, 1973; Garstang and Betts, 1974; Grant and Lock, 2004; Heus et al., 2009b; Neggers et al., 2007).”***

MC3) I have some major concerns about the analysis framework.

MC3.1) One of my main concerns is that the theoretical arguments lean heavily on analysis of adiabatic parcels, with mixing as an afterthought. Previous studies suggest that adiabatic parcels do not occur in shallow and congestus cumulus (e.g. Romps and Kuang, 2010), and this seems to be the case in the current study as well. Note that liquid water path is plotted on a logarithmic scale, i.e. even the clouds that contain most liquid water contain several times less liquid water than they would in the adiabatic case. An adiabatic parcel model therefore offers only very limited insight into the dynamics of cumulus convection. Several approaches exist that better represent the effects of mixing throughout the cloud life cycle, e.g. continuous lateral entrainment (Lin and Arakawa 1997, Morrison 2017) or episodic mixing. In order for a theoretical framework to provide quantitative predictions that can be tested against LES, one would likely need such an approach. Moreover, it is clear from a number of recent publications (De Roode et al. 2012 is cited already, but see also Romps and Charn, 2015; Morrison, 2016) that theoretical models for the vertical velocity should incorporate the role of drag.

MA3.1) As expressed in MA1, the original manuscript was faulty in that it gave an impression that it focused on entrainment effects. So we have revised the manuscript to better explain that the theoretical estimations of entrainment effects only serve to give an intuitive understanding of the results found using LES simulations. We use simple dynamical concepts to explain the evolutions of the different core types in cumulus clouds. As written now in the beginning of the theoretical section: "***Here we propose simple physical considerations to evaluate the differences in cloud partition to core and margin using different definitions. The arguments rely on key findings from previous works (see Sect. 1) with aim to gain intuitive understanding of the potential differences between the core types***".

We are well aware that the use of an adiabatic cloud column (as done in the theoretical part) is simplistic, nevertheless, we think it manages to easily convey theoretical ideas and robust cloud field characteristics, such as convective overshooting. For the cloud field analyses (using the CvM phase space), the adiabatic curve is taken as a reference for the growth stage of clouds. We find that it makes it very helpful when trying to extract temporal information from those figures, as was shown in previous publications (Heiblum et al., 2016a, 2016b).

Regarding the importance of drag on vertical velocity, we address this point in the introduction: ***"Usually, the CAPE serves as a theoretical upper limit, and the vertical velocity is smaller due to multiple effects (de Roode et al., 2012), most importantly the perturbation pressure gradient force (which oppose the air motion) and mixing with the environment (entrainment/detrainment) (de Roode et al., 2012; Morrison, 2016a; Peters, 2016). Recent studies have shown that entrainment effects on vertical velocity are of second order, and a rising thermal shows a balance between buoyancy and the perturbation pressure gradient (Hernandez-Deckers and Sherwood, 2016; Romps and Charn, 2015), the latter acting as a drag force on the updrafts. Nevertheless, initial updraft magnitude and environmental conditions play a crucial role in determining the magnitude of mixing effects on buoyancy, and thus also the vertical velocity profile in the cloud (Morrison, 2016a, 2016b, 2017)."***.

And in the theoretical section:

"***Given an initial vertical velocity of ~ 0.5 m/s, the deceleration due to buoyancy (and reversal to negative vertical velocity) should occur within a typical time range of 1 - 10 minutes. These timescales are much longer than the typical timescales of entrainment (mixing and evaporation that eliminate the B_{core}) which range between***

1 – 10 s (Lehmann et al., 2009). Moreover, the fact that a drag force typically balances the buoyancy acceleration (Romps and Charn, 2015) can also contribute to a time lag between effects on buoyancy and subsequent effects on vertical velocity. Therefore, the switching of sign for vertical velocity should occur with substantial delay compared to the reduction of buoyancy, and B_{core} should be a subset of W_{core} (i.e. $B_{core} \subseteq W_{core}$) during the growing and mature stages of a cloud's lifetime.”

Nevertheless, we note that our goal in the paper is not to develop a new parameterization for vertical velocity or gain new insights on the different components of the vertical velocity equation, but rather to get a general understanding of the processes affecting each core type.

MC3.2) The use of the liquid water path as a measure of cloud mass also seems more appropriate for stratocumulus than for cumulus convection, where clouds may be slanted and mixing might lead to lateral growth. Referring to the mean liquid water path as the cloud mass is confusing. Instead of liquid water path, a tracer concentration could be used (e.g. Romps and Kuang, 2010) to provide a more robust measure of dilution.

MA3.2) The use of mean liquid water path (LWP) as a measure of cloud mass is an inherent property of the CvM phase space. The center of gravity (COG) which is taken as the vertical coordinate, can be easily linked to the LWP by using the theoretical case of adiabatic cloud column. So there is a good reference case. In addition we note that the mean LWP is taken by dividing the total mass by the mean cross-sectional area, so that even if clouds are slanted the mean LWP will reflect a “slanted” column. Using here the CvM phase space, as was done for cumulus cloud fields in previous works (Heiblum et al., 2016a, 2016b) enables examination of all clouds, at all stages of lifetime for the entire simulation. So we chose to use the CvM phase space due to its suitability to our purposes while we explain its advantages and limitations in the text: “***In this space, the Center-of-Gravity (COG) height and mass of each cloud in the field at each output time step (taken here to be 1 min) are collected and projected in the CvM phase space. This enables a compact view of all clouds in the simulation during all stages of their lifetimes, with the main disadvantage being the loss of grid-size resolution information on in-cloud dynamical processes***”.

MC3.3) The analysis in this study mostly considers convective elements as a whole, or fractions of pixels within an element (figure 2 is an exception here). This provides limited insight into the dynamics of the different cores. Previous studies have provided a more detailed analysis into the circulation around rising cumulus clouds (see, e.g. Blyth et al, 2005; Peters, 2016). Considering the different regions identified in these previous studies would be another way to obtain novel results that go beyond the current conclusions.

MA3.3) We agree with the reviewer that the insights into in-cloud core dynamics is limited. However, as explained in depth above, this is not part of the objectives of this work. We choose to perform a general comparison between the three core types for large statistics of clouds rather than increase the understanding of core dynamics.

MC3.4) The thresholds used in the analysis should be discussed further. One of the risks of only considering zero thresholds is that passive regions of the cloud with marginal updraught velocities or regions where gravity waves lead to upwards motion are included in the analysis. Some previous studies have addressed this issue by looking into streamlines (e.g. Romp and Charn, 2015), however, this might not be very straightforward to implement. Alternative approaches would be to determine characteristic updraught values of buoyancy and vertical velocity, or considers multiple thresholds.

MA3.4) The issue of which threshold to choose for the different core types occupied us a great deal. Indeed, choosing a >0 threshold includes passive regions with marginal updrafts increases the variance of the results for the small dissipating clouds. In Fig. RA1 we show the sensitivity to the different threshold for the single cloud case. Increasing the Wcore threshold significantly affects its extent. We find that up to w>0.15, the Wcore remains the largest, but for higher thresholds RHcore tends to be the largest.

Nevertheless, we think the >0 threshold is the only one which is purely physical. All other thresholds are case dependent and can change considerably from case to case. For a study aiming to analyze specific cloud dynamical features it might make sense to apply a strict threshold and limit the variance. But for a comparison we find that the current threshold is the most general. This point is now discussed in the revised text:

"***We note that setting the core thresholds to positive values (>0) may increase the amount of non-convective pixels which are classified as part of a physical core, especially for the W_{core}. Indeed, taking higher thresholds for the updrafts decreases the W_{core} extent and reduces the variance. Nevertheless, any threshold taken is subjective in nature, while the positive vertical velocity definition is process based and objective.***"

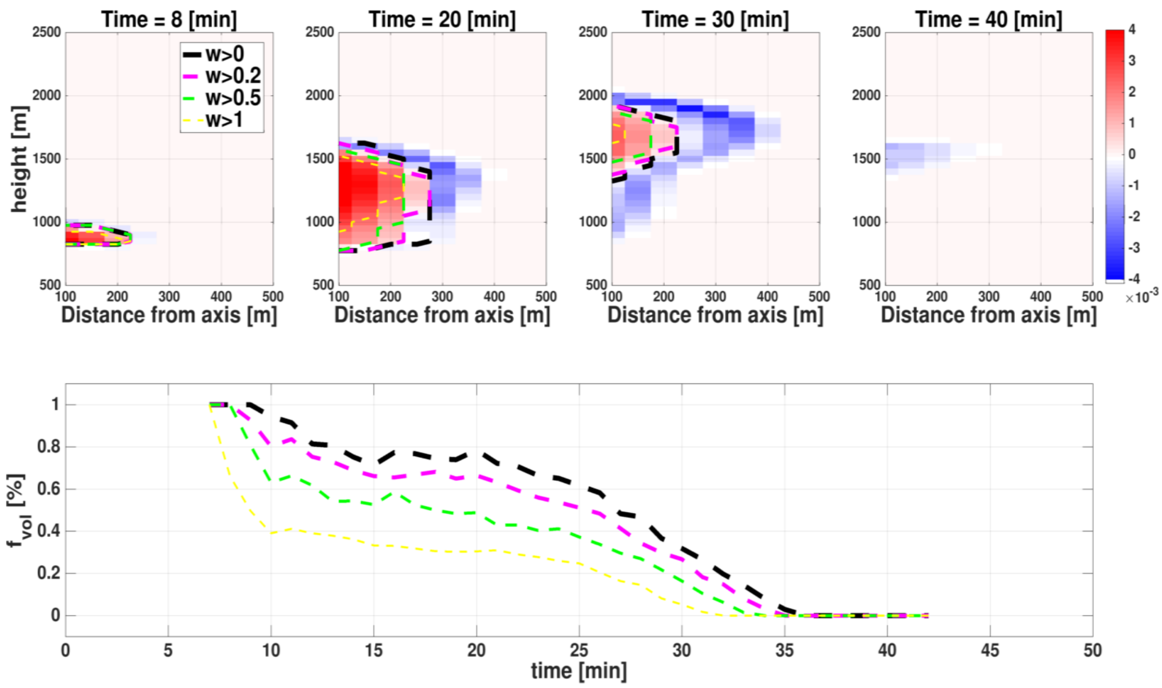

Fig. RA1. Top: Four vertical cross-sections (at t=8, 20, 30, 40 minutes) during the single cloud simulation with aerosol concentration of 500 CCN. Y-axis represents height [m] and X-axis represents the distance from the axis [m]. The black, magenta, green and yellow dashed lines represent different vertical velocity core thresholds (see legend for values). The background represents the condensation (red) and evaporation rate (blue) [g kg^{-1} s^{-1}]. Bottom: Temporal evolution of vertical velocity core volume fractions (using different thresholds) from the total cloud volume (f_{vol}).

MC3.5) The domain used may be too small for the Amazon simulations. In order to check this, one would need to check that the cloud top is sufficiently far removed from the domain top, and that convective cold pools are not dominating the spatial organization of convection.

MA3.5) Thank you for this comment. After reexamination of the Amazon simulations we found that indeed cold pools play a dominant role in the organization of the cloud field. Therefore we decided to change the manuscript and show a newer and more documented case study (CASS - http://portal.nersc.gov/project/capt/CASS/).

The revised section about Cloud field model (section 2.2): ***"To check the robustness of the cloud field results, two additional case studies are simulated: (1) The same Hawaiian profile used to initiate the single cloud model, and (2) a continental shallow cumulus convection cases study (named CASS), based on long term observations taken at the ARM Southern Great Plains (SGP) site (Zhang et al., 2017)."***

This continental case study produced similar results to the oceanic case studies in the paper as can be seen in the revised fig. 7 below.

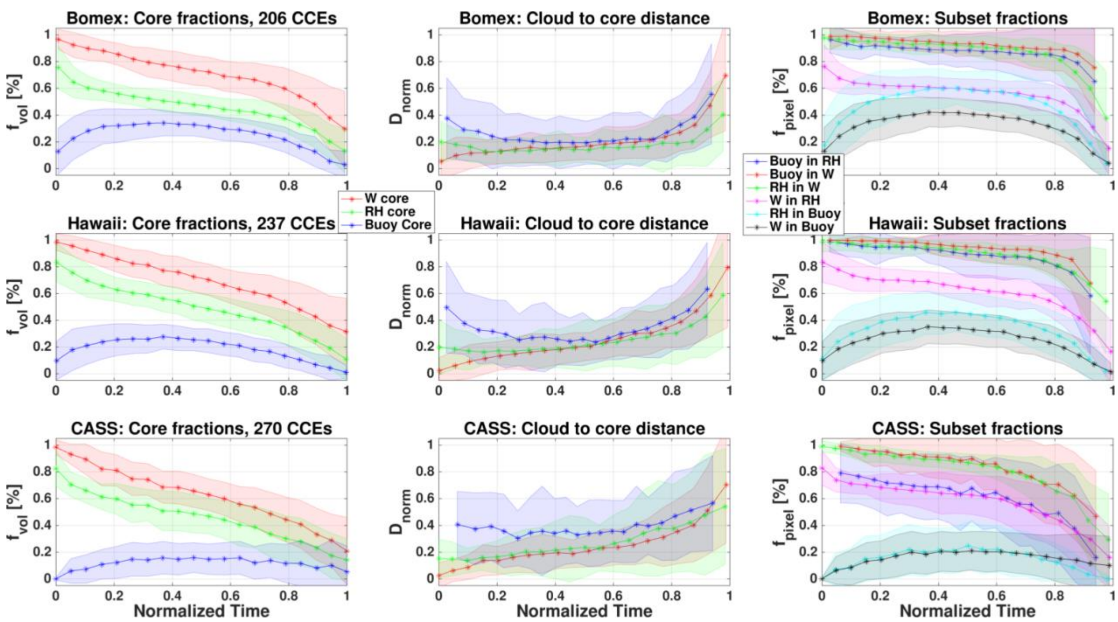

Figure 7 (from the revised manuscript). Normalized time series of CCE averaged core fractions for the BOMEX (upper row), Hawaii (middle row), and CASS (bottom row) simulations. Both core volume fractions (f_{vol}, left column), normalized distances between cloud and core centroid locations (D_{norm}, middle column), and pixel fractions of one core within another (f_{pixel}, right column) are considered. Line colors indicated different core types (see legends), while corresponding shaded color regions indicate the standard deviation. Normalized time enables to average together CCEs with different lifetimes, from formation to dissipation. The number of CCEs averaged together for each simulation is included in the left column panel titles.

Specific comments:

SC1) Equation 2 seems to be based on a parcel that is not mixing with its environment (see my main concern 1 above).

SA1) Equation 2 is added here to provide a non-expert with a basic understanding of how supersaturation and vertical velocity are thermodynamically linked. For the sake of accuracy, we have clarified that equation 2 (eq. 3 in new manuscript) refers to the adiabatic case which neglects mixing: "***Neglecting mixing with the environment, S and w can be linked as follows:***

$$\frac{dS}{dt} = Q_1 w - Q_2 \frac{dq_l}{dt} \qquad (3),$$

where Q_1, Q_2 ***are thermodynamic factors (Rogers and Yau, 1989)***."

SC2) The presentation style of figures needs improvement. For example, in figure 2, some of the contours overlap, which makes the current presentation confusing to the reader. Some figures are also too small in my opinion (figure 2 is an example here).

SA2) Thank you for this comment. All of the figures were redone so that the texts are larger, features are clearer, and cases where lines overlap can be distinguished. Figure 2 is added here for example:

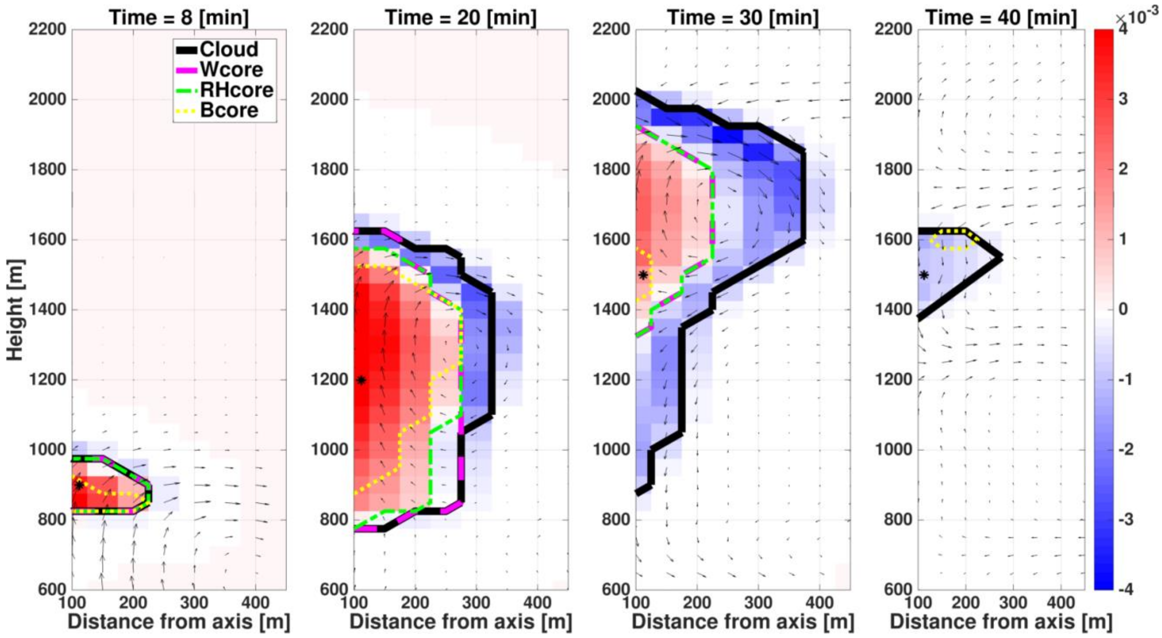

Figure 2 (from manuscript). Four vertical cross-sections (at t=8, 20, 30, 40 minutes) during the single cloud simulation. Y-axis represents height [m] and X-axis represents the distance from the axis [m]. The black, magenta, green and yellow lines represent the cloud, W_{core}, RH_{core} and B_{core}, respectively. The black arrows represent the wind, the background represents the condensation (red) and evaporation rate (blue) [g kg^{-1} s^{-1}], and the black asterisks indicate the vertical location of the cloud centroid. Note that in some cases the lines indicating core boundaries overlap (mainly seen for RH and W cores).

SC3) Equations should avoid the use of acronyms, such as LWC (in any case, is this specific humidity or mixing ratio?)

SA3) Thank you for this comment, we have replaced LWC with q_l – liquid water mixing ratio in eq. 3 (see SA1 above), and eq. 1, as follows:

$$B = g \cdot \left(\frac{\theta'}{\theta_o} + 0.61 q_v' - q_l\right) \qquad (1).$$

SC4) Some of the terminology is unclear: are cloud growth/cloud suppression regions simply regions of net increase/decrease of supersaturation, or is something beyond this meant? It is important to point out that some of the regions that are subsaturated using a bin microphysics scheme would be diagnosed as saturated in an approach to condensation which performs immediate adjustment when defining the RH-core. Similarly, buoyancy is best defined with respect to the surrounding environment, rather than with respect to a reference profile.

SA4) Thank you for noticing this. We have added to the revised text exact definition of cloud growth in the introduction: "…***partitioned to two main regions: i) a core region, where mainly cloud growth processes occur (i.e. condensation – accumulation of cloud mass), and…***", the single cloud results: "***During cloud growth (i.e. (increase in mass and size)…***", and cloud field results: "…***fractions decrease with cloud growth (increase in mass and COG height) while…***".

In addition, we point out in the text the importance of bin-microphysics that enables cases of sub-saturated cloudy pixels: "***It should be noted that the bin-microphysical schemes used here calculate saturation explicitly, by solving the diffusion growth equation, enabling super- and sub- saturation values in cloudy pixels. This is in contrary to many other works that used bulk-microphysical schemes which rely on saturation adjustment to 100% within the cloud (Khain et al., 2015). This difference may produce significant differences on the evolution of clouds and their cores*** ".

Finally, as suggested by the reviewer the buoyancy is taken with respect to the surrounding environment. Citing from the text: "$\boldsymbol{B_{core}}$***: buoyancy (see definition in Eq. (1)) above zero. The buoyancy is determined in each time step by comparing each cloudy pixel with the mean thermodynamic conditions for all non-cloudy pixels per vertical height***".

SC5) Parentheses should only be used around the year when an author is cited and the author name is part of the sentence.

SA5) Thank you, this issue has been addressed.

SC6) I could not find the reference to Dias et al. (2012). I have not done a comprehensive check for other missing references at this point.

SA6) This reference is no longer relevant and has been removed from the text.

<u>Reply to reviewer #2 –RC2</u>

General Reviewer Comment

The work herein seeks to examine and compare three methods of defining convective cores through analysis of buoyancy (B), relative humidity (RH), and vertical velocity (W). The authors do a thorough job of comparing and contrasting the evolution of the various core definitions and highlight the overlap or lack thereof among the 3 defining core characteristics. They have performed their analysis via multiple methods including a theoretical model, single column type model, and a couple of models at the LES scale with bin microphysics and without saturation adjustment assumptions which can be limiting. The results appear quite robust among all methods of representing convective clouds and their cores and among various thermodynamic environments represented by different initial soundings. The manuscript is well-written, clear and concise, but a few questions and concerns, given below, should be addressed.

General Answer: We thank the reviewer for the beneficial comments and we were happy to read that the reviewer found our results robust and the paper well written and clear. The manuscript was revised according to all the comments.

Main Comments:

MC1) The motivation of the paper seems to lack its proper placement with respect to previous published work regarding convective cores and entrainment. While the focus of this work is specific to examining the relative differences between core definitions and their evolution over time, the work should be more appropriately placed in context and should emphasize what is novel in this work.

MA1) Thank you for this comment. In the revised manuscript clear emphasis is put on the novel parts of this work: the differences between the three core types, their evolutions in time, and comparison to previous understanding of core size and location within a cloud. In addition, the introduction was changed significantly to include a broader review of works and ideas from the past that are relevant to this work.

We have added a few sentences to the introduction that clarify the objectives of the work: "***Specifically, we aim to answer questions such as:***

- ***Which core type is largest? Which is smallest?***
- ***How do the cores change during the lifetime of a cloud?***
- ***Can different core types be used interchangeably without much effect on analysis results?***
- ***Are the cores centered at the cloud' geometrical center, as expected from the core-shell model?"***

MC2) Some aspects of this work regarding entrainment, dilution, and their impacts on buoyancy are not new. However, the framework of comparing cores, core subsets, and their evolution in multiple model frameworks is perhaps more unique. It may help to better frame the paper in such a light.

MA2) Thank you for this comment. The abstract, introduction, and summary in the revised manuscript now put more emphasis on the novelties of the work while referring better to previous works when relevant. Although previous works have dealt with positive vertical velocity and buoyancy in clouds and the effects of entrainment on them, we do not know of a work which tries to perform a comprehensive comparison between the different cores and tracks these cores throughout their lifetime. The new abstract now focuses on these aspects of the work:

"The properties of a warm convective cloud are determined by the competition between the growth and dissipation processes occurring within it. One way to observe and follow this competition is by partitioning the cloud to core and margin regions. Here we look at three core definitions: positive vertical velocity (W_{core}), supersaturation (RH_{core}), and positive buoyancy (B_{core}), and follow their evolution throughout the lifetime of warm convective clouds.

Using single cloud and cloud field simulations with bin-microphysics schemes, we show that the different core types tend to be subsets of one another in the following order: $B_{core} \subseteq RH_{core} \subseteq W_{core}$. This property is seen for several different thermodynamic profile initializations, and is generally maintained during the

growing and mature stages of a cloud's lifetime. This finding is in line with previous works and theoretical predictions showing that cumulus clouds may be dominated by negative buoyancy at certain stages of their lifetime.

During its mature growth stage, the cloud and its cores are centered at a similar location. During cloud dissipation the cores show less overlap, typically reduce in size, and migrate from the cloud centroid. In some cases, buoyancy cores can reemerge and often reside at the cloud periphery. Thus, the core-shell model of a positively buoyant center surrounded by negatively buoyant shell only applies to a fraction of the cloud lifetime.”

Specific Comments:

SC1) Line 40: Here you mention that negatively buoyant cloud may exist due to $W>0$ and $S>1$. You might specifically mention the other components of the W equation that keep $W>0$ and $S>1$ and their relative contributions during stages of $B>0$ and $B<0$. Perhaps this could also be addressed in the main text in greater detail. Once $B<0$, the other components of the W equation will begin to weaken since the “fuel” is missing. What tends to weaken faster, and what implications does this have for the W core?

SA1) This part was removed from the revised abstract. The existence of negatively buoyant clouds (as referred to in the previous version) can be attributed to inertia or “leftover fuel from sub-cloudy layer buoyancy. The other components of the vertical velocity equation (de Roode et al., 2012; Romps and Charn, 2015) can only decelerate the buoyant updrafts and not actually create a cloud. An exception is large scale advection and quasi-geostrophic ascent, which are irrelevant to the scope of this paper. Many previous works have dealt with the relative importance and feedbacks of the W equation components (de Roode et al., 2012; Morrison, 2016a, 2016b; Romps and Charn, 2015) and we think it is a subject that requires a study on its own. However, we revised the paper to better explain the W equation in the introduction, as follows:

“***Neglecting cases of air flow near obstacles or air mass fronts, buoyancy is the main source for vertical momentum in the cloud. In its simplest form, the vertical velocity (w) in the cloud can be approximated by the convective available potential energy***

(CAPE) of the vertical column up to that height (Rennó and Ingersoll, 1996; Williams and Stanfill, 2002; Yano et al., 2005):

$$\mathbf{0.5w^2(h) = \int_{h_0}^{h} B(z)\,dz = CAPE(h)} \qquad \textit{(2).}$$

Here we define CAPE to be the vertical integral of buoyancy from the lowest level of positive buoyancy (h_0, initiation of vertical velocity) to an arbitrary top height (h). Usually, the CAPE serves as a theoretical upper limit, and the vertical velocity is smaller due to multiple effects (de Roode et al., 2012), most importantly the perturbation pressure gradient force (which oppose the air motion) and mixing with the environment (entrainment/detrainment) (de Roode et al., 2012; Morrison, 2016a; Peters, 2016). Recent studies have shown that entrainment effects on vertical velocity are of second order, and a rising thermal shows a balance between buoyancy and the perturbation pressure gradient (Hernandez-Deckers and Sherwood, 2016; Romps and Charn, 2015), the latter acting as a drag force on the updrafts."

SC2) Lines 177: The potential initial temperature perturbation of 1C is rather large for this type of shallow convection setup. Could such a large perturbation shock the initial field and generate a sizeable convective pulse and gravity waves that impacts the rather small domain size?

SA2) Thank you for this comment. There was a mistake in the text. The SAM model was initialized with random ±0.1°C (instead of ±0.1-1°C) perturbations throughout the domain. It is corrected in the revised text.

SC3) Line 182: The cloud pixel threshold here of 0.01g/kg seems rather small. What could be deemed a visible cloud would likely be closer to 0.1g/kg. Including values closer to 0.01g/kg would likely include very diffuse clouds at cloud edges that are generated in models. Choosing a different threshold could seemingly have a great impact on the definition of the cloud volume. Have you examined the impact of this threshold choice? I am aware that many papers have used the 0.01 g/kg threshold; but the choice here seems more critical given the examination of cloud volume and such.

SA3) The question of cloud pixel liquid water content (LWC) threshold is something we have examined as part of this work. We started by taking an even lower threshold of 0.005 g/kg (Cohen and Craig, 2006) but eventually raised the threshold to 0.01 g/kg based on other works (Jiang et al., 2009; Xue and Feingold, 2006). The impact of threshold choice is shown in Fig. RB1 below. The 0.01 and 0.005 g/kg thresholds yield similar results with regards to cloud volume, while higher thresholds (0.05 and 0.1 g/kg) reduce cloud volume significantly. By taking areas of condensation and evaporation as indicators of cloudy regions, it can be seen that the higher values thresholds “miss” pixels with high evaporation rate (vapor diffusion), in both growing and dissipating stages of cloud lifetime. Hence, we find that the 0.01 g/kg threshold best reflects a cloudy volume, without the risk of including insignificant cloud debris as can be seen in some cases for the lower 0.005 g/kg threshold.

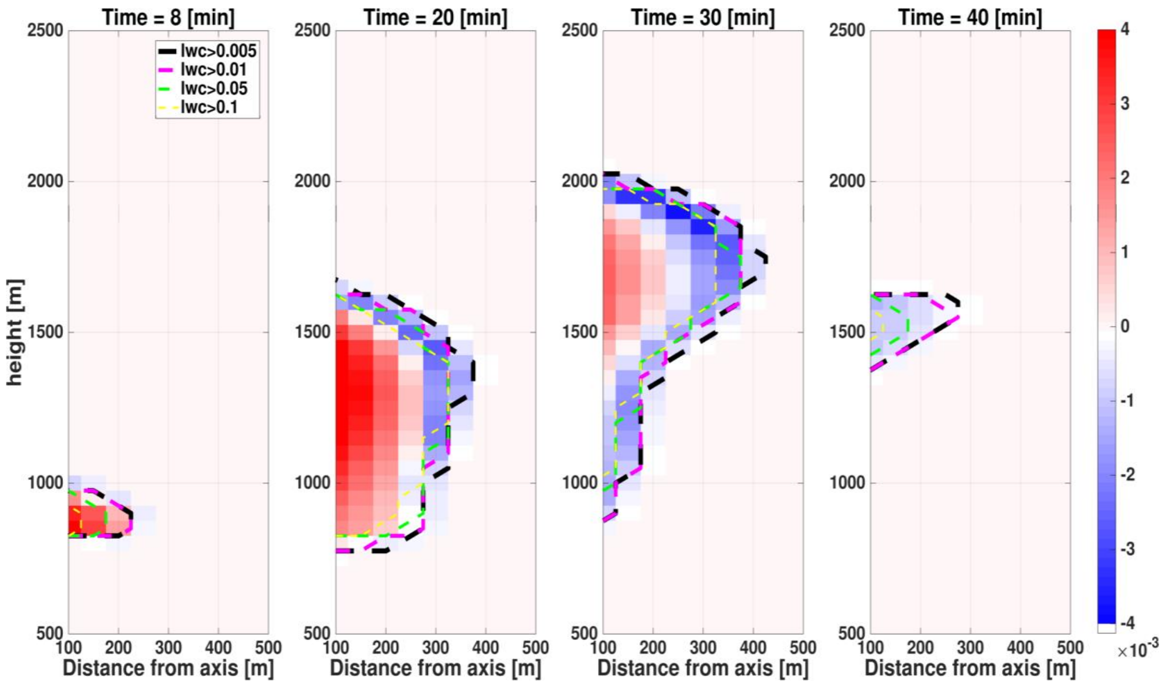

Fig. RB1. Four vertical cross-sections (at t=8, 20, 30, 40 minutes) during the single cloud simulation with aerosol concentration of 500 CCN. Y-axis represents height [m] and X-axis represents the distance from the axis [m]. The black, magenta, green and yellow dashed lines represent different LWC thresholds for a cloudy pixel (see legend for values). The background represents the condensation (red) and evaporation rate (blue) [g kg^{-1} s^{-1}].

SC4) Line 184-186: Here you state that buoyancy is determined relative to the mean thermodynamic conditions for non-cloud pixels. How is buoyancy computed and applied in the dynamic core of the model? Are these the same or different, and what are the implications if these are different?

SA4) The buoyancy in the dynamical core of the axisymmetric model is calculated in a similar way to the buoyancy calculations as described in the paper, with the sole difference being the dynamical core buoyancy is calculated with respect to the mean initial thermodynamic conditions while we take the mean instantaneous non-cloudy thermodynamic conditions. Since the domain is sufficiently large and unaffected during the simulation, the differences between the two buoyancy calculations is negligible, as can be seen in Fig. RB2.

In the cloud field model (SAM) the dynamical core buoyancy is calculated with respect to the mean horizontal thermodynamic conditions (cloudy and non-cloudy), which gives almost identical results to our calculation in this work (i.e. with respect to only non-cloudy).

Since each of the models' dynamical core calculates buoyancy a bit differently, we chose one calculation that applies to both.

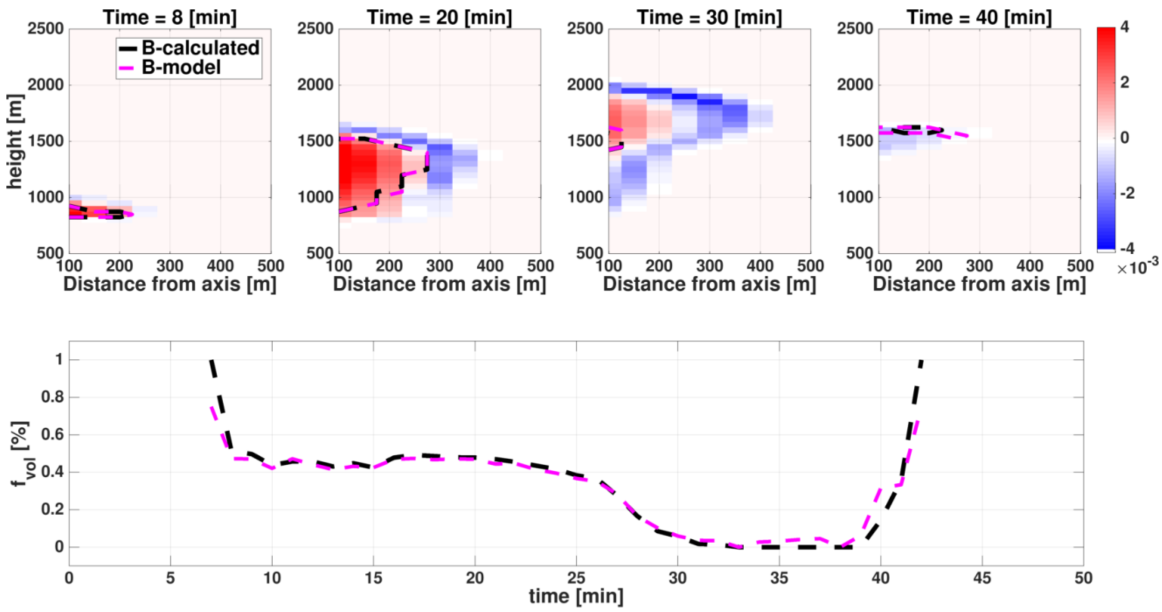

Fig. RB2. Comparison of dynamical core buoyancy (magenta lines) with calculated buoyancy (black lines). The top panels are similar to Fig. RB1, but with lines representing core extent. The bottom panel shows the temporal evolution of buoyancy core volume fraction from the total cloud volume (f_{vol}).

SC5) Line 257: Here you state that the cloud top downdraft promotes adiabatic heating that leads to the decay phase positive buoyancy. Is this definitive or supposition here? Is this seen in other clouds? Is this adiabatic heating greater than any local evaporative cooling?

SA5) A significant part of Part II of this work was devoted to the explanation of why pockets of positive buoyancy appear is non-convective regions of dissipating clouds. We show that if the evaporative cooling is weak enough (or no evaporation occurs), the adiabatic heating is sufficient to create positive buoyancy in weak downdrafts. The reader is referred to Part II within the text for the single cloud:
"***Further analysis (see Part II) shows that the entire dissipating cloud is colder and more humid than the environment but downdrafts from the cloud top (see arrows in Fig. 2) promote adiabatic heating, and by that increase the buoyancy in dissipating cloudy pixels, sometimes reaching positive values. These buoyant pockets will be discussed further in Part II.*** ".
and cloud field:
"***The prevalence of cloud edge B_{core} pixels during dissipation can be explained by adiabatic heating due to weak downdrafts (see Sect. 4.2, Part II) which are expected at the cloud periphery***.".

SC6) Line 268-270: Are the changes in cloud volume fraction susceptible to the choice of cloud mass concentration used to define a cloud grid cell (0.01 g/kg)? How would choosing a different threshold impact your analysis?

SA6) We have tested this question as part of this work and found that the main conclusions would not have changed regardless of the LWC threshold chosen. This fact is demonstrated in Fig. RB3 for the single cloud case, where it can be seen that the subset properties of the three cores and their relative sizes are similar. The main difference that arises is the positive buoyancy core that appears during dissipation only for lower cloud LWC thresholds. However, we find this effect to be substantial in the cloud field simulation and for other aerosol concentrations, and thus should not be considered an outlier only seen for very low LWC pixels. An additional figure for a low aerosol concentration of 25 CCN is also shown below (Fig. RB4), where an increase in buoyancy core during dissipation is seen for all thresholds.

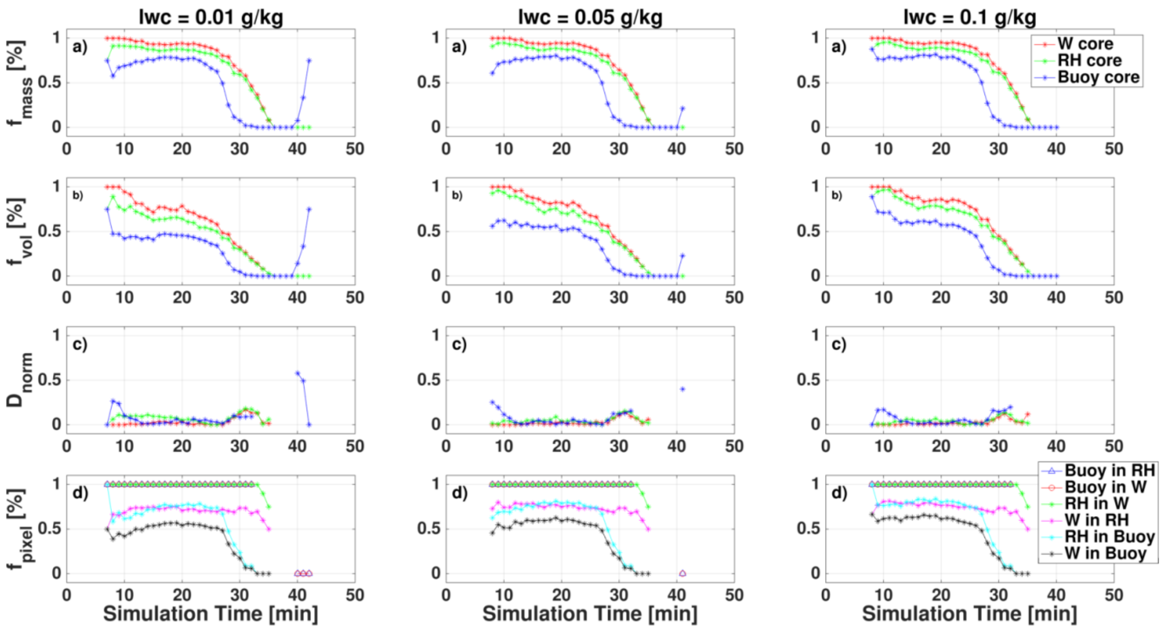

Fig. RB3. Same as figure 3 in the manuscript, but for three different cloudy pixel LWC thresholds [g/kg]: 0.01 (left column), 0.05 (middle column), 0.1 (right column). Aerosol concentration is 500 CCN.

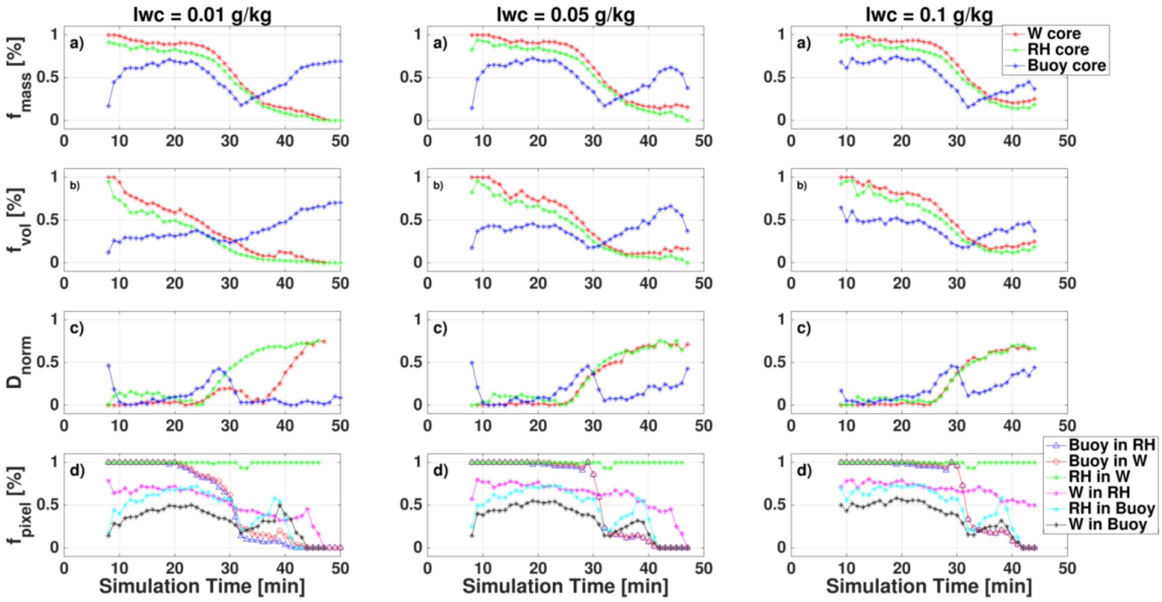

Fig. RB4 Same as figure RB3, but for an aerosol concentration of 25 CCN.

SC7) Line 722: How valid is this non-changing temperature assumption to your analysis?

This seems like a rather unrealistic and constricting assumption. The local dT could be large which could greatly impact dB and mixing.

SA7) The non-changing temperature assumption only applies to the reference environmental temperature. This assumption is based on the fact that the environment is sufficiently large and its mean temperature is not affected by local evaporation. We find this assumption to be standard practice for almost all models calculating buoyancy (Khairoutdinov and Randall, 2003; Seigel, 2014), which take the horizontal mean temperature as reference (which changes very slowly during the course of a simulation, if at all), rather than a local temperature in the vicinity of a cloud.

SC8) Line 267: "expect" should be "except".
SA8) Thank you, the change was carried out.

SC9) Line 371: "overweighs" should be "outweighs".
SA9) Thank you, the change was carried out.

SC10) Line 591: "cloud's" should be "clouds".
SA10) Thank you, the typo was fixed

SC11) Line 619: "from precipitation" should be "by precipitation".
SA11) Thank you, the change was carried out.

SC12) Line 634: This should read: "In cases where the: : :."
SA12) Thank you, we added "where" to the sentence.

SC13) Figures: My main comment about the figures is that most of them need to be larger, especially the fonts, so that they are easily readable. The time series plots need to be much large in order to see overlap where it exists.
SC13) Thank you for this comment. All of the figures were redone so that the texts are larger and cases where lines overlap can be distinguished.

References

de Roode, S. R.: Thermodynamics of cumulus clouds, Física de la Tierra; Vol 19 (2007), 2008.

de Roode, S. R. and Bretherton, C. S.: Mass-Flux Budgets of Shallow Cumulus Clouds, J. Atmos. Sci., 60(1), 137–151, doi:10.1175/1520-0469(2003)060<0137:MFBOSC>2.0.CO;2, 2003.

de Roode, S. R., Siebesma, A. P., Jonker, H. J. J. and de Voogd, Y.: Parameterization of the vertical velocity equation for shallow cumulus clouds, Mon. Wea. Rev., 140(8), 2424–2436, doi:10.1175/MWR-D-11-00277.1, 2012.

de Rooy, W. C. and Siebesma, A. P.: A simple parameterization for detrainment in shallow cumulus, Mon. Wea. Rev., 136(2), 560–576, doi:10.1175/2007MWR2201.1, 2008.

Betts, A. K.: Non-precipitating cumulus convection and its parameterization, Q.J Royal Met. Soc., 99(419), 178–196, doi:10.1002/qj.49709941915, 1973.

Cohen, B. G. and Craig, G. C.: Fluctuations in an equilibrium convective ensemble. part II: numerical experiments, J. Atmos. Sci., 63(8), 2005–2015, doi:10.1175/JAS3710.1, 2006.

Derbyshire, S. H., Maidens, A. V., Milton, S. F., Stratton, R. A. and Willett, M. R.: Adaptive detrainment in a convective parametrization, Q.J Royal Met. Soc., 137(660), 1856–1871, doi:10.1002/qj.875, 2011.

Emanuel, K. A.: A Scheme for Representing Cumulus Convection in Large-Scale Models, J. Atmos. Sci., 48(21), 2313–2329, doi:10.1175/1520-0469(1991)048<2313:ASFRCC>2.0.CO;2, 1991.

Garstang, M. and Betts, A. K.: A review of the tropical boundary layer and cumulus convection: structure, parameterization, and modeling, Bull. Amer. Meteor. Soc., 55(10), 1195–1205, doi:10.1175/1520-0477(1974)055<1195:AROTTB>2.0.CO;2, 1974.

Grant, A. L. M. and Lock, A. P.: The turbulent kinetic energy budget for shallow cumulus convection, Q.J Royal Met. Soc., 130(597), 401–422, doi:10.1256/qj.03.50, 2004.

Gregory, D. and Rowntree, P. R.: A Mass Flux Convection Scheme with Representation of Cloud Ensemble Characteristics and Stability-Dependent Closure, Mon. Wea. Rev., 118(7), 1483–1506, doi:10.1175/1520-0493(1990)118<1483:AMFCSW>2.0.CO;2, 1990.

Heiblum, R. H., Altaratz, O. and Koren, I.: Characterization of cumulus cloud fields using trajectories in the center of gravity versus water mass phase space: 1. Cloud tracking and phase space description, Journal of …, 2016a.

Heiblum, R. H., Altaratz, O. and Koren, I.: Characterization of cumulus cloud fields using trajectories in the center of gravity versus water mass phase space: 2. Aerosol effects on warm convective clouds, Journal of …, 2016b.

Hernandez-Deckers, D. and Sherwood, S. C.: A numerical investigation of cumulus thermals, J. Atmos. Sci., 73(10), 4117–4136, doi:10.1175/JAS-D-15-0385.1, 2016.

Heus, T., J. Pols, C. F., J. Jonker, H. J., A. Van den Akker, H. E. and H. Lenschow, D.: Observational validation of the compensating mass flux through the shell around cumulus clouds, Q.J Royal Met. Soc., 135(638), 101–112, doi:10.1002/qj.358, 2009a.

Heus, T. and Jonker, H. J. J.: Subsiding Shells around Shallow Cumulus Clouds, J. Atmos. Sci., 65(3), 1003–1018, doi:10.1175/2007JAS2322.1, 2008.

Heus, T., Jonker, H. J. J., Van den Akker, H. E. A., Griffith, E. J., Koutek, M. and Post, F. H.: A statistical approach to the life cycle analysis of cumulus clouds selected in a virtual reality environment, J. Geophys. Res., 114(D6), doi:10.1029/2008JD010917, 2009b.

Jiang, H., Feingold, G. and Koren, I.: Effect of aerosol on trade cumulus cloud morphology, J. Geophys. Res., 114(D11), doi:10.1029/2009JD011750, 2009.

Jonker, H. J. J., Heus, T. and Sullivan, P. P.: A refined view of vertical mass transport by cumulus convection, Geophys. Res. Lett., 35(7), doi:10.1029/2007GL032606, 2008.

Kain, J. S. and Fritsch, J. M.: A One-Dimensional Entraining/Detraining Plume Model and Its Application in Convective Parameterization, J. Atmos. Sci., 47(23), 2784–2802, doi:10.1175/1520-0469(1990)047<2784:AODEPM>2.0.CO;2, 1990.

Khain, A. P., Beheng, K. D., Heymsfield, A., Korolev, A., Krichak, S. O., Levin, Z., Pinsky, M., Phillips, V., Prabhakaran, T., Teller, A., van den Heever, S. C. and Yano, J. I.: Representation of microphysical processes in cloud-resolving models: Spectral (bin) microphysics versus bulk parameterization, Rev. Geophys., 53(2), 247–322, doi:10.1002/2014RG000468, 2015.

Khairoutdinov, M. F. and Randall, D. A.: Cloud resolving modeling of the ARM summer 1997 IOP: model formulation, results, uncertainties, and sensitivities, J. Atmos. Sci., 60(4), 607–625, doi:10.1175/1520-0469(2003)060<0607:CRMOTA>2.0.CO;2, 2003.

Lehmann, K., Siebert, H. and Shaw, R. A.: Homogeneous and inhomogeneous mixing in cumulus clouds: Dependence on local turbulence structure, Journal of the Atmospheric Sciences, 66(12), 3641–3659, 2009.

Morrison, H.: Impacts of updraft size and dimensionality on the perturbation pressure and vertical velocity in cumulus convection. part I: simple, generalized analytic solutions, J. Atmos. Sci., 73(4), 1441–1454, doi:10.1175/JAS-D-15-0040.1, 2016a.

Morrison, H.: Impacts of updraft size and dimensionality on the perturbation pressure and vertical velocity in cumulus convection. part II: comparison of theoretical and numerical solutions and fully dynamical simulations, J. Atmos. Sci., 73(4), 1455–1480, doi:10.1175/JAS-D-15-0041.1, 2016b.

Morrison, H.: An analytic description of the structure and evolution of growing deep cumulus updrafts, J. Atmos. Sci., 74(3), 809–834, doi:10.1175/JAS-D-16-0234.1, 2017.

Neggers, R. A. J., Stevens, B. and Neelin, J. D.: Variance scaling in shallow-cumulus-topped mixed layers, Q.J Royal Met. Soc., 133(628), 1629–1641, doi:10.1002/qj.105, 2007.

Paluch, I. R.: The entrainment mechanism in colorado cumuli, J. Atmos. Sci., 36(12), 2467–2478, doi:10.1175/1520-0469(1979)036<2467:TEMICC>2.0.CO;2, 1979.

Peters, J. M.: The Impact of Effective Buoyancy and Dynamic Pressure Forcing on Vertical Velocities within Two-Dimensional Updrafts, J. Atmos. Sci., 73(11), 4531–4551, doi:10.1175/JAS-D-16-0016.1, 2016.

Rennó, N. O. and Ingersoll, A. P.: Natural convection as a heat engine: A theory for CAPE, J. Atmos. Sci., 53(4), 572–585, doi:10.1175/1520-0469(1996)053<0572:NCAAHE>2.0.CO;2, 1996.

Rodts, S. M. A., Duynkerke, P. G. and Jonker, H. J. J.: Size Distributions and Dynamical Properties of Shallow Cumulus Clouds from Aircraft Observations and Satellite Data, J. Atmos. Sci., 60(16), 1895–1912, doi:10.1175/1520-0469(2003)060<1895:SDADPO>2.0.CO;2, 2003.

Rogers, R. R. and Yau, M. K.: A Short Course in Cloud Physics, Butterworth Heinemann, Burlington, MA., 1989.

Romps, D. M. and Charn, A. B.: Sticky Thermals: Evidence for a Dominant Balance between Buoyancy and Drag in Cloud Updrafts, J. Atmos. Sci., 72(8), 2890–2901, doi:10.1175/JAS-D-15-0042.1, 2015.

Seigel, R. B.: Shallow Cumulus Mixing and Subcloud-Layer Responses to Variations in Aerosol Loading, J. Atmos. Sci., 71(7), 2581–2603, doi:10.1175/JAS-D-13-0352.1, 2014.

Taylor, G. R. and Baker, M. B.: Entrainment and detrainment in cumulus clouds, J. Atmos. Sci., 48(1), 112–121, doi:10.1175/1520-0469(1991)048<0112:EADICC>2.0.CO;2, 1991.

Wang, Y., Geerts, B. and French, J.: Dynamics of the cumulus cloud margin: an observational study, J. Atmos. Sci., 66(12), 3660–3677, doi:10.1175/2009JAS3129.1, 2009.

Williams, E. and Stanfill, S.: The physical origin of the land–ocean contrast in lightning activity, Comptes Rendus Physique, 3(10), 1277–1292, doi:10.1016/S1631-0705(02)01407-X, 2002.

Xue, H. and Feingold, G.: Large-Eddy Simulations of Trade Wind Cumuli: Investigation of Aerosol Indirect Effects, J. Atmos. Sci., 63(6), 1605–1622, doi:10.1175/JAS3706.1, 2006.

Yano, J.-I., Chaboureau, J.-P. and Guichard, F.: A generalization of CAPE into potential-energy convertibility, Q.J Royal Met. Soc., 131(607), 861–875, doi:10.1256/qj.03.188, 2005.

Zhang, Y., Klein, S. A., Fan, J., Chandra, A. S., Kollias, P., Xie, S. and Tang, S.: Large-Eddy Simulation of Shallow Cumulus over Land: A Composite Case Based on ARM Long-Term Observations at Its Southern Great Plains Site, J. Atmos. Sci., 74(10), 3229–3251, doi:10.1175/JAS-D-16-0317.1, 2017.

Core and margin in warm convective clouds. Part I: core types and evolution during a cloud's lifetime

[1]Reuven H. Heiblum, [1]Lital Pinto, [1]Orit Altaratz, [1,2]Guy Dagan, [1]Ilan Koren

[1]Department of Earth and Planetary Sciences, Weizmann Institute of Science, Rehovot, Israel

[2] now at: Atmospheric, Oceanic and Planetary Physics, Department of Physics, University of Oxford, UK

Corresponding Email – ilan.koren@weizmann.ac.il

Abstract

The properties of a warm convective cloud are determined by the competition between the growth and dissipation processes occurring within it. One way to observe and follow this competition is by partitioning the cloud to core and margin regions. Here we look at three core definitions: positive vertical velocity (W_{core}), supersaturation (RH_{core}), and positive buoyancy (B_{core}), and follow their evolution throughout the lifetime of warm convective clouds.

Using single cloud and cloud field simulations with bin-microphysics schemes, ~~W~~we show that the different core types tend to be ~~proper~~ subsets of one another in the following order: $B_{core} \subseteq RH_{core} \subseteq W_{core}$. ~~Using single cloud and cloud field simulations, we find that t~~This property is seen for several different thermodynamic profile initializations, and is generally maintained during the growing and mature stages of a cloud's lifetime~~, but can break down during the dissipation stage~~. This finding is in line with previous works and theoretical predictions showing that cumulus clouds may be dominated by negative buoyancy at certain ~~all~~ stages of their lifetime.

During its mature and growth stage, ~~T~~the cloud and its cores are centered at a similar location. ~~, while d~~During cloud dissipation the cores show less overlap, typically reduce in size, and migrate from the cloud centroid. In some cases, buoyancy cores can reemerge and often ~~may~~ reside at the cloud periphery. Thus, the core-shell model of a positively buoyant center surrounded by negatively buoyant shell only applies to a fraction of the cloud lifetime.

~~A theoretical model is developed, showing that in both the adiabatic and non-adiabatic cases, B_{core} can be expected to be the smallest core, due to two main reasons: i) entrainment rapidly decreases the buoyancy core compared to the other core types, and ii) convective clouds may exist while being completely negatively buoyant (while maintaining positive vertical velocity and supersaturation).~~

1. Introduction

Clouds are important players in the climate system (Trenberth et al., 2009), and currently constitute one of the largest uncertainties in climate and climate change research (IPCC, 2013). One of the reasons for this large uncertainty is the complexity created by opposing processes that occur at the same time but in different locations within a cloud. Although a cloud is generally considered as a single entity, physically, it can be partitioned to two main regions: i) a core region, where mainly cloud growth processes occur (i.e. condensation - accumulation of cloud mass), and ii) a margin region, where cloud suppression processes occur (i.e. evaporation - loss of cloud mass). Changes in thermodynamic or microphysical (aerosol) conditions impact the processes in both regions (sometimes in different ways), and thus the resultant total cloud properties (Dagan et al., 2015). To better understand cloud properties and their evolution in time, it is necessary to understand the interplay between physical processes within the core and margin regions (and the way they are affected by perturbations in the environmental conditions).

Considering convective clouds, there are several ~~parameters~~ objective measures that ~~are commonly~~have been used in previous works for separating a cloud's core from its margins (will be referred to as physical cores hereafter). ~~Previous works have used these objective measures to define a cloud core (with the margins defined as the remaining regions of the cloud).~~ In deep convective cloud simulations the core is usually defined by the updrafts' magnitude using a certain threshold, usually W>1 $m \cdot s^{-1}$ (Khairoutdinov et al., 2009; Kumar et al., 2015; Lebo and Seinfeld, 2011; Morrison, 2012). Studies on warm cumulus clouds ~~studied the main parameters that affect warm cumulus clouds vertical velocity and~~have defined the clouds' core as parts with positive buoyancy and positive updrafts (de Roode et al., 2012; Dawe and Austin, 2012; Heus and Jonker, 2008; Siebesma and Cuijpers, 1995)~~.~~ or solely regions with positively buoyancy (Heus and Seifert, 2013; Seigel, 2014). More recently, cloud partition to regions of supersaturation and sub-saturation has been used to define the cloud core in single cloud simulations (Dagan et al., 2015).

For simplicity, we focus ~~here~~ on warm convective clouds (only contain liquid water), avoiding the additional complexity and uncertainties associated with mixed phase and ice phase microphysics. The common assumption when partitioning a convective cloud to its physical core and margin is that the cloud core is at its geometrical center ~~is its core~~ and the peripheral regions (i.e. edges) are the margin. Previous observational (Heus et al., 2009a; Rodts et al., 2003; Wang et al., 2009) and numerical (Heus and Jonker, 2008; Jonker et al., 2008; Seigel, 2014) works have studied the gradients of cloud thermodynamic properties from cloud center to edge, and suggest that a cloud is best described by a core-shell model. This model assumes a core with positive vertical velocity and buoyancy, surrounded by a shell with negative vertical velocity and buoyancy. The shell is the region where mixing between cloudy and environmental air parcels occurs, leading to evaporative cooling → decrease in buoyancy → decrease in vertical velocity.

Based on previous ~~works~~findings, here we explore the partition of clouds to core and margin using three different objective core definitions where the cloud core threshold is set to be a positive value (of buoyancy, vertical velocity, or supersaturation). Cloud buoyancy (B) ~~(which is the driving force for convection) is one of the intuitive parameters used and~~ can be approximated by the following formula:

$$B = g \cdot \left(\frac{\theta'}{\theta_o} + 0.61 q_v' - q_l\right) \qquad (1),$$

Where θ_o represents the reference state potential temperature, q_v is the water vapor mixing ratio, and ~~LWC~~ q_l is the liquid water content. The (') stands for the deviation from the reference state per height (Wang et al., 2009). Buoyancy is a measure for the vertical acceleration and its integral is the convective potential energy~~, or the fuel that drives cloud growth~~. Latent heat release during moist adiabatic ascent fuels positive buoyancy and clouds' growth, while evaporation and subsequent cooling drives cloud decay (de Roode, 2008; Betts, 1973). The ~~existence~~prevalence of negatively buoyancy parcels at the cloud edges due to mixing and evaporation is a well-known phenomena (Morrison, 2017). Mixing diagrams have been used to assess this effect (de Roode, 2008; Paluch, 1979; Taylor and Baker, 1991), and are at the root of convective parameterization schemes (Emanuel, 1991; Gregory and Rowntree, 1990; Kain and Fritsch, 1990) and parameterizations of entrainment and detrainment in cumulus clouds (de Rooy and Siebesma, 2008; Derbyshire et al., 2011).

Neglecting cases of air flow near obstacles or air mass fronts, buoyancy is the main source for vertical momentum in the cloud. In its simplest form, the vertical velocity

(w) in the cloud can be approximated by the convective available potential energy (CAPE) of the vertical column up to that height (Rennó and Ingersoll, 1996; Williams and Stanfill, 2002; Yano et al., 2005):

$$0.5w^2(h) = \int_{h_0}^{h} B(z)\,dz = CAPE(h) \qquad (2).$$

Here we define CAPE to be the vertical integral of buoyancy from the lowest level of positive buoyancy (h_0, initiation of vertical velocity) to an arbitrary top height (h). Usually, the CAPE serves as a theoretical upper limit, and the vertical velocity is smaller due to multiple effects (de Roode et al., 2012), most importantly the perturbation pressure gradient force (which oppose the air motion) and mixing with the environment (entrainment/detrainment) (de Roode et al., 2012; Morrison, 2016a; Peters, 2016). Recent studies have shown that entrainment effects on vertical velocity ~~can be neglected~~are of second order, and a rising thermal shows a balance between buoyancy and the perturbation pressure gradient (Hernandez-Deckers and Sherwood, 2016; Romps and Charn, 2015), the latter acting as a drag force on the updrafts. Nevertheless, initial updraft and environmental conditions play a crucial role in determining the magnitude of mixing effects on buoyancy, and thus also the vertical velocity profile in the cloud (Morrison, 2016a, 2016b, 2017).

The supersaturation (S, where S=1 is 100% relative humidity) core definition (S-1>0 or RH>100%) partitions the cloud core and margin to areas of condensation and evaporation. Since we consider convective clouds~~ here~~, the only driver of supersaturation during cloud growth is upward vertical motion of air.~~ Thus, the vertical velocity core partitions the cloud to areas where the saturation ratio increases (upward motion) or decreases (downward motion). The vertical velocity (w) and the supersaturation (S, where S=1 is 100% relative humidity) can also be used for defining a cloud core,core.~~ Neglecting mixing with the environment, ~~they~~ S and w can be~~and are~~ linked as follows:

$$\frac{dS}{dt} = Q_1 w - Q_2 \frac{d\sout{LWC}q_l}{dt} \qquad (3),$$

where Q_1,Q_2 are thermodynamic factors (Rogers and Yau, 1989). The thermodynamic factors are nearly insensitive to pressure for temperature above 0°C, and both weakly decrease (less than 15% net change) with temperature increase between 0°C and 30°C

(Pinsky et al., 2013). The first term on the right-hand side is related to the change in the supersaturation due to adiabatic cooling or heating of the moist air (due to vertical motion). The second term is related to the change in the supersaturation due to condensation/evaporation of water vapor/drops. Hence, the supersaturation in a rising parcel depends on the magnitude of the updraft and on the condensation rate of vapor to drops (a sink term). The latter is proportional to the concentration of aerosols in the cloud (Reutter et al., 2009; Seiki and Nakajima, 2014), which serve as cloud condensation nuclei (CCN) for cloud droplets. In Part II of this work we demonstrate some of the insights gained by investigating differences between the different cores properties and their time evolution when changing the aerosol loading.

The ~~goals~~ purpose of this part of the work (part I) are to compare and understand the differences between the three basic definitions of cloud core (i.e. $W_{core}, RH_{core}, B_{core}$) throughout a convective cloud's lifetime, using both theoretical arguments and numerical simulations. It should be noted that the bin-microphysical schemes used here calculate saturation explicitly, by solving the diffusion growth equation, enabling super- and sub- saturation values in cloudy pixels. This is in contrary to many other works that used bulk-microphysical schemes which rely on saturation adjustment to 100% within the cloud (Khain et al., 2015). This difference may produce significant differences on the evolution of clouds and their cores. Specifically, we aim to answer questions such as:

- Which core type is largest? Which is smallest?
- How do the cores change during the lifetime of a cloud?
- Can different core types be used interchangeably without much effect on analysis results?
- Are the cores centered around the cloud' geometrical center, as expected from the core-shell model?

The differences between the cores' evolution in time shed new light on the competition of processes within a cloud in time and space. Moreover, such an understanding can serve as a guideline to all studies that perform the partition to cloud core and margin, and assist in determining the relevance of a given partition.

2. Methods

2.1. Single cloud model

For single cloud simulations we use the Tel-Aviv University axisymmetric, non-hydrostatic, warm convective single cloud model (TAU-CM). It includes a detailed (explicit) treatment of warm cloud microphysical processes solved by the multi-moment bin method (Feingold et al., 1988, 1991; Tzivion (Tzitzvashvili) et al., 1989; Tzivion et al., 1994). The warm microphysical processes included in the model are nucleation, diffusion (i.e. condensation and evaporation), collisional coalescence, breakup and sedimentation (for a more detailed description, see (Reisin et al., 1996)).

Convection was initiated using a thermal perturbation near the surface. A time step of 1 sec is chosen for dynamical computations, and 0.5 sec for the microphysical computations (e.g. condensation-evaporation). The total simulation time is 80 min. There are no radiation processes in the model. The domain size is 5x6 km, with an isotropic 50 m resolution. The model is initialized using a Hawaiian thermodynamic profile, based on the 91285 PHTO Hilo radiosonde at 00Z, 21 Aug, 2007. A typical oceanic size distribution of aerosols is chosen (Altaratz et al., 2008; Jaenicke, 1988), with a total concentration of 500 cm^{-3}. This concentration produced clouds that are non- to weakly- precipitating. In Part II additional aerosol concentrations are considered, including ones which produce heavy precipitation.

2.2. Cloud field model

Warm cumulus cloud fields are simulated using the System for Atmospheric Modeling (SAM) Model (version 6.10.3, for details see webpage: http://rossby.msrc.sunysb.edu/~marat/SAM.html) (Khairoutdinov and Randall, 2003)). SAM is a non-hydrostatic, anelastic model. Cyclic horizontal boundary conditions are used together with damping of gravity waves and maintaining temperature and moisture gradients at the model top. An explicit Spectral Bin Microphysics (SBM) scheme (Khain et al., 2004) is used. The scheme solves the same warm microphysical processes as in the TAU-CM single cloud model, and uses an identical aerosol size distribution and concentration (i.e. 500 cm^{-3}) for the droplet activation process.

We use the BOMEX case study as our benchmark for shallow warm cumulus fields. This case simulates a trade-wind cumulus (TCu) cloud field based on observations made near Barbados during June 1969 (Holland and Rasmusson, 1973). This case study has a well-established initialization setup (sounding, surface fluxes, and surface roughness) and large scale forcing setup (Siebesma et al., 2003). It has been thoroughly tested in many previous studies (Grabowski and Jarecka, 2015; Heus et al., 2009b; Jiang and Feingold, 2006; Xue and Feingold, 2006). To check the robustness of the cloud field results, two additional case studies are simulated: (1) The same Hawaiian profile used to initiate the single cloud model, and (2) an Amazonian warm cumulus case based on the afternoon dry season mean profile for August 2001 obtained during the Large-scale Biosphere-Atmosphere (LBA) experiment data at Belterra, Brazil (Dias et al., 2012).

All three soundings (BOMEX, Hawaiian, and Amazonian) and surface properties used to initialize the model are detailed in (Heiblum et al., 2016a) . The grid size is set to 100 m in the horizontal direction and 40 m in the vertical direction for all simulations. The domain size is 12.8 km x 12.8 km x 4 km for the BOMEX simulation and extends to 5 km, 6 km in the vertical direction for the Hawaii and Amazon simulations, respectively. The time step for computation is 1 s for all simulations, with a total runtime of 8 hours. The initial temperature perturbations (randomly chosen within ± 0.1-1 ºC) are applied near the surface, during the first time step.

2.3. Physical and Geometrical Core definitions

A cloudy pixel is defined here as a grid-box with liquid water amount that exceeds 0.01 g kg^{-1}. The physical core of the cloud is defined using three different definitions: 1) RH_{core}: all grid boxes for which the relative humidity (RH) exceeds 100%, 2) B_{core}: buoyancy (see definition in Eq. (1)) above zero. The buoyancy is determined in each time step by comparing each cloudy pixel with the mean thermodynamic conditions for all non-cloudy pixels per vertical height, and 3) W_{core}: vertical velocity above zero. These definitions apply for both the single cloud and cloud field model simulations used here. We note that setting the core thresholds to positive values (>0) may increase the amount of non-convective pixels which are classified as part of a physical core, especially for the W_{core}. Indeed, taking higher thresholds for the updrafts decreases the

W_{core} extent and reduces the variance. Nevertheless, any threshold taken is subjective in nature, while the positive vertical velocity definition is process based and objective. ~~Additional thresholds have also been checked for the updrafts or buoyancy definitions, yielding similar conclusions.~~

The centroid (i.e. mean location in each of the axes) is used here to represent the geometrical location of the total cloud (i.e. cloud geometrical core) and its specific physical cores. The distances between the total cloud and its cores' centroids (D_{norm}), as presented here, are normalized to cloud size to reflect the relative distance between the two centroids, where $D_{norm} = 0$~~0~~ indicates coincident physical and geometrical cores and $D_{norm} = 1$ ~~1~~ indicates a physical core located at the cloud boundary. The single cloud simulations rely on an axisymmetric model and thus all centroids are horizontally located on the center axis while vertical deviations are permitted. For this model the distance is normalized by half the cloud's thickness. For the cloud field simulations both horizontal and vertical deviations are possible, therefore distances are normalized by the cloud's volume radius.

2.4. Center of gravity vs. Mass (CvM) phase space

Recent studies (Heiblum et al., 2016a, 2016b) suggested the Center-of-Gravity vs. Mass (CvM) phase space as a useful approach to reduce the high dimensionally and to study results of large statistics of clouds during different stages of their lifetimes (such as seen in cloud fields). In this space, the Center-of-Gravity (COG) height and mass of each cloud in the field at each output time step (taken here to be 1 min) are collected and projected in the CvM phase space. This enables a compact view of all clouds in the simulation during all stages of their lifetimes. Although the scatter of clouds in the CvM is sensitive to the microphysical and thermodynamic settings of the cloud field, it was shown that the different subspaces in the CvM space correspond to different cloud processes and stages (Heiblum et al., 2016a, 2016b). The lifetime of a cloud can be described by a trajectory on this phase space.

A schematic illustration of the CvM space in shown in Fig. 1. Most clouds are confined between the adiabat (curved dashed line) and the inversion layer base (horizontal dashed line). The adiabat curve corresponds to the theoretical evolution of a moist adiabat 1D cloud column in the CvM space. The large majority of clouds form within the growing branch (yellow shade) at the bottom left part of the space, adjacent to the adiabat. Clouds then follow the growing trajectory (grow in both COG and mass) to some maximal values. The growing branch deviates from the adiabat at large masses depending on the degree of sub-adiabaticity of the cloud field. After or during the growth stage of clouds, they may undergo the following processes: i) dissipate via a reverse trajectory along the growing one, ii) dissipate via a gradual dissipation trajectory (magenta shade), iii) shed off small mass cloud fragments (red shades), iv) in the case of precipitating clouds, they can shed off cloud fragments in the sub-cloudy layer (grey shade). The former two processes form continuous trajectories in the CvM space, while the latter two processes create disconnected subspaces.

2.5. Cloud tracking

To follow the evolution of individual clouds within a cloud field we use an automated 3D cloud tracking algorithm (see (Heiblum et al., 2016a) for details). It enables tracking of Continuous Cloud Entities (CCEs) from formation to dissipation, even if interactions between clouds (splitting or merging) occur during that lifetime. A CCE initiates as a new cloud forming in the field, and is tracked on the condition that it retains the majority (>50%) of its mass during an interaction event if occurs. Thus, a CCE can terminate due to either cloud dissipation or cloud interactions.

3. Theoretical estimations for different core sizes~~considerations explaining the single cloud simulation results~~

Here we propose simple physical considerations ~~that~~ ~~predict~~ to evaluate the ~~simulated~~ differences in cloud partition to core and margin using different definitions. The arguments rely on key findings from previous works (see Sect. 1) with aim to ~~summarize our present understanding~~gain intuitive understanding of the potential differences between the core types. It is convenient to separate the analysis to an adiabatic case, and then add another layer of complexity and consider the effects of mixing of cloudy and non-cloudy air. In this theoretical derivation saturation adjustment to RH=100% is assumed for both cases, while in the other models used in this study transient super- and sub-saturated cloudy parcels are treated (more realistic).

3.1. Adiabatic case – no mixing

~~For the case of an adiabatic cloud column~~Considering moist-adiabatic ascent, the excess vapor above saturation is instantaneously converted to liquid (saturation adjustment). Thus, the adiabatic cloud is saturated (S=1) throughout its vertical profile, and only W_{core} and B_{core} differences can be considered. It is assumed that the adiabatic convective cloud is initiated by positive buoyancy initiating from the sub-cloudy layer. As long as the cloud is growing it should have positive CAPE and will experience positive w throughout the column even if the local buoyancy at specific height is negative. Eventually the cloud must decelerate due to negative buoyancy and reach a top height, where CAPE = 0 and $w = 0$. Hence, for the adiabatic column case, B_{core} is always a proper subset of W_{core} ($B_{core} \subset W_{core}$). These effects are commonly seen in warm convective cloud fields where permanent vertical layers of negative buoyancy (but with updrafts) within clouds typically exist at the bottom and top regions of the cloudy layer (de Roode and Bretherton, 2003; Betts, 1973; Garstang and Betts, 1974; Grant and Lock, 2004; Neggers et al., 2007).

3.2. Cloud parcel entrainment model

A mixing model between a saturated (cloudy) parcel and a dry (environment) parcel is used to illustrate the effects of mixing on the different core types. The details of these theoretical calculations are shown in Appendix A. The initial cloudy parcel is assumed to be saturated (part of RH_{core}), have positive vertical velocity (part of W_{core}), and experience either positive or negative buoyancy (part of B_{core} or B_{margin}), as is seen for the adiabatic column case. Additionally, mixing is assumed to be isobaric, and in a steady environment where the average temperature of the environment per a given height does not change. The resultant mixed parcel will have lower humidity content and lower LWC as compared to the initial cloudy parcel, and a new temperature. In nearly all cases (beside in an extremely humid environment) the mixed parcel will be sub-saturated and evaporation of LWC will occur. Evaporation ceases when equilibrium is reached due to air saturation (S=1) or due to complete evaporation of the droplets (which means S<1, and the mixed parcel is no longer cloudy since it has no liquid water content).

In addition to mixing between cloudy (core or margin) and non-cloudy parcels, mixing between core and margin parcels (within the cloud) also occurs. This mixing process can be considered as "entrainment-like" with respect to the cloud core. Considering the changes in the W_{core} and RH_{core}, there is no fundamental difference in the treatment of mixing of cloudy and non-cloudy parcels, or mixing between core and margin (because the margins and the environment are typically sub-saturated and experience negative vertical velocity). However, for the changes in the B_{core} after mixing, there exists a fundamental difference between mixing *with* the reference temperature/humidity state (in the case of mixing with the environment) and mixing *given* a reference temperature/humidity state (in mixing between B_{core} and B_{margin}). Thus, it is interesting to check the effects of mixing between B_{core} and B_{margin} parcels on the total extent of the B_{core} with respect to the other two core types. The details of this second case are shown in Appendix B.

3.2.1. Effects of non-cloudy entrainment on buoyancy

When mixed with non-cloudy air, the change in buoyancy of the initial cloudy parcel (which is a part of W_{core} and RH_{core} and either B_{core} or B_{margin}) happens due to both mixing and evaporation processes. The theoretical calculations show that for all relevant temperatures (~0°C to 30°C, representing warm Cu), the change in the parcel's buoyancy due to evaporation alone will always be negative (see appendix A). It is because the negative effect of the temperature decrease ~~overweighs~~ outweighs the positive effects of the humidity increase and water loading decrease. Nevertheless, the total change in the buoyancy (due to both mixing and evaporation) depends on the initial temperature, relative humidity, and liquid water content of the cloudy and non-cloudy parcels.

In Fig. A1 a wide range of non-cloudy environmental parcels, each with their own thermodynamic conditions, are mixed with a saturated cloud parcel with either positive or negative buoyancy. The main conclusions regarding the effects of such mixing on the buoyancy are as follows:

i. To a first order, the initial buoyancy values are temperature dependent, where a cloudy parcel that is warmer (colder) by more than ~ 0.2°C than the environment will be positively (negatively) buoyant for common values of cloudy layer environment relative humidity (RH>80%).

ii. Parcels that are initially part of B_{core} may only lower their buoyancy due to entrainment, either to positive or negative values depending on the environmental conditions.

iii. The lower the environmental RH, the larger the probability for parcel transition from B_{core} to B_{margin} after entrainment.

iv. Parcels that are initially part of B_{margin} can either increase or decrease their buoyancy value, but never become positively buoyant. The former case (buoyancy decrease) is expected be more prevalent since it occurs for the smaller range of temperature differences with the environment.

In summary, entrainment is expected to always have a net negative effect on B_{core} extent and B_{margin} values, while evaporation feedbacks serve to maintain RH_{core} in the cloud. Thus, we can predict that B_{core} should be a subset of RH_{core} (i.e. $B_{core} \subseteq RH_{core}$).

3.2.2. Effects of core and margin mixing on buoyancy

We consider the case of mixing between the B_{core} and $B_{margin,}$ meaning positively buoyant and negatively buoyant cloud parcels. For simplicity, we assume both parcels are saturated (S=1, both included in the RH_{core}). As seen above, such conditions exist in both the adiabatic case and in the case where an adiabatic cloud has undergone some entrainment with the environment. The buoyancy differences between the saturated parcels are mainly due to temperature differences, but also due to the increasing saturation vapor pressure with increasing temperature (see Appendix B for details).

In Fig. B1 is it shown that the resultant mixed parcel's buoyancy can be either positive or negative, depending on the magnitude of temperature difference of each parcel (core or margin) from that of the environment. However, in all cases the mixed parcel is supersaturated. This result can be generalized: given two parcels with equal RH but different temperature, the RH of the mixed parcel is always equal or higher than the initial value. Hence, B_{core} can either increase or decrease in extent, while the RH_{core} can only increase due to mixing between saturated B_{core} and B_{margin} parcels. This again strengthens the assumption that B_{core} should be a subset of RH_{core}.

We note that an alternative option for mixing between the core and margin parcels that exist here, where either or both of the parcels are subsaturated so that the mixed parcel is subsaturated as well. In this case evaporation will also occur. As seen in Appendix A, this should further reduce the buoyancy value of the mixed parcel (while increasing the RH).

3.2.3. Effects of entrainment on vertical velocity

~~We divide the entrainment effects on the W_{core} to two: i) a direct effect which includes conservation of momentum of vertical velocity between the core and margin/non-cloudy parcels, and ii) an indirect effect of vertical velocity changes due to buoyancy changes caused by the entrainment.~~The vertical velocity equation dictates that buoyancy is the main production term (de Roode et al., 2012; Romps and Charn, 2015), and is balanced by perturbation pressure gradients and mixing (on grid and sub-grid scales). Thus, all changes of magnitude (and sign) in vertical velocity should lag the changes in buoyancy. This is the basis of convective overshooting and cumulus formation in the transition layer (see Sect. 3.1). It is interesting to assess the magnitude of this effect by quantifying the expected time lag between buoyancy and vertical velocity changes. ~~The direct effect can be considered to occur instantaneously.(de Roode et al., 2012) Assuming homogeneous mixing of both parcels and a mixing fraction of 0.5, the direct effect can be simplified to conservation of momentum before and after mixing. Since both parcels are approximately of equal mass (in isobaric mixing), the mixed parcel's vertical velocity will be the average of the initial velocities. If the absolute value of the updraft in the W_{core} parcel is larger than that of the~~

~~downdraft in the margin/non-cloudy parcel, the resultant mixed parcel will remain part of W_{core}. This is usually the case during the growing stages in clouds, where it can be assumed that the surrounding air around W_{core} is at rest or with downdrafts weaker than the updrafts within the W_{core}.~~

~~As opposed to the direct effect, the indirect effect is time dependent.~~ The calculations in Appendix A indicates negative buoyancy values reaching -0.1 m/s^2 due to entrainment. However, measurements from within clouds show that the temperature deficiency of cloudy parcels with respect to the environment is generally restricted to less than 1^{o}C for cumulus clouds (Burnet and Brenguier, 2010; Malkus, 1957; Sinkevich and Lawson, 2005; Wei et al., 1998), and thus the negative buoyancy should be no more larger than -0.05 m/s^2. This value is closer to current and previous simulations and also observations that show negative buoyancy values within clouds to be confined between -0.001 and -0.01 m/s^2 (de Roode et al., 2012; Ackerman, 1956). Given an initial vertical velocity of ~ ~~1~~ 0.5 m/s, the deceleration due to buoyancy (and reversal to negative vertical velocity) should occur within a typical time range of 1 - 10 minutes. These timescales are much longer than the typical timescales of entrainment (mixing and evaporation that eliminate the B_{core}) which range between 1 – 10 s (Lehmann et al., 2009). Therefore, ~~even if entrainment acts to reduce~~the switching of signs of vertical velocity~~, it does so with~~ should occur with substantial delay compared to the reduction of buoyancy, and B_{core} should be a subset of W_{core} (i.e. $B_{core} \subseteq W_{core}$) during the growing and mature stages of a cloud's lifetime.

3.3. The relation between supersaturation and vertical velocity cores

Here we revisit the terms in Eq. 3. A rising parcel initially has no liquid water content, with its only source of supersaturation being the updraft w, and thus initially the RH_{core} should always be a ~~proper~~ subset of W_{core}. In general, since the sink term $\frac{dLWC}{dt}$ becomes a source only when S<1 (the condition for evaporation), the only way for a convective cloud to produce supersaturation (i.e. S>1) is by updrafts during all stages of its lifetime. Once supersaturation is achieved, the sink term becomes positive $\frac{dLWC}{dt} >$ 0 and balances the updraft source term, so that supersaturation either increases or decreases. At any stage, if downdrafts replace the updrafts within a supersaturated parcel, the consequent change in supersaturation becomes strictly negative (i.e. $\frac{dS}{dt} < 0$). This negative feedback limits the possibility to find supersaturated cloudy parcels with downdrafts. Hence, we can expect the RH_{core} to be smaller than W_{core}~~, even though not necessarily a proper subset.~~ during the majority of a cloud’s lifetime.

4~~3~~. Results - Single cloud simulation

The differences between the three types of core definitions are examined during the lifetime of a single cloud (Fig. 2), based on the Hawaiian profile. The cloud's total lifetime is 36 minutes (between t=7 and t=43 min of simulation). Each panel in Fig. 2 presents vertical cross-sections of the three cores (magenta - W_{core}, green - RH_{core}, and yellow - B_{core}) at four points in time (with 10-minute intervals). The cloud has an initial cloud base at 850m, and grows to a maximal top height of 2050 m. The condensation rates (red shades) increase toward the cloud center and the evaporation rates (blue shades) increase toward the cloud edges. Evaporation at the cloud top results in a large eddy below it that contributes to mixing and evaporation at the lateral boundaries of the cloud. Thus, a positive feedback is initiated which leads to cooling, negative buoyancy, and downdrafts. The dissipation of the cloud is accompanied with a rising cloud base and lowering of the cloud top.

During the growing stage (t=10, 20 min), when substantial condensation still occurs within the cloud, all of the cores seem to be self-contained within one another, with B_{core} being the smallest and W_{core} being the largest. During the final dissipation stages, when the cloud shows only evaporation (t=40), W_{core} and RH_{core} disappear while there is still a small B_{core} near the cloud top. Further analysis shows that the entire dissipating cloud is colder and more humid than the environment but downdrafts from the cloud top (see arrows in Fig. 2) promote adiabatic heating, and by that increase the buoyancy in dissipating cloudy pixels, sometimes reaching positive values. These buoyant pockets will be discussed further in Part II. The results indicate that the three types of physical cores of the cloud are not located around the cloud’s geometrical core along the whole cloud lifetime. During cloud growth (i.e. (increase in mass and size) the three types of cores surround the cloud's center, while during late dissipation the B_{core} is at offset from the cloud center.

For a more complete view of the evolution of the three core types in the single cloud case, time series of core fractions are shown in Fig. 3. Panels a and b show the core mass (core mass / total mass - f_{mass}) and volume (core volume / total volume - f_{vol}) fractions out of the cloud's totals. The results are similar for both measures ~~expect~~ except for the fact that core mass fractions are larger than core volume fractions. This is due to significantly higher LWC per pixel in the cores compared to the margins, which skews the core mass fraction to higher values. Core mass fractions during the main cloud growing stage (between t=7 and t=27 min simulation time) are around 0.7 - 0.85 and core volume fractions are around 0.5 - 0.7. The time series show that as opposed to the W_{core} and RH_{core} fractions which decrease monotonically with time, B_{core} shows a slight increase during stages of cloud growth. In addition, for most of the cloud's lifetime the B_{core} fractions are the smallest and the W_{core} fractions are the largest, except for the final stage of the clouds dissipation where downdrafts from the cloud top creates pockets of positive buoyancy. These pockets are located at the cloud's peripheral regions rather than near the cloud's geometrical center as is typically expected for the cloud's core. In the cloud's center (the geometrical core) the B_{core} is the first one to terminate (at t=32 min) compared to both $W_{core}$and RH_{core} that decay together (at 36 min).

For describing the locations of the physical cores, we examine the normalized distances (D_{norm}) between the cloud's centroid and the cores' centroids. The evolution of these distances is shown in Fig. 3c. At cloud initiation (t=7 min), when the cloud is very small, all cores' centroids coincide with the total cloud centroid location. The B_{core} (and RH_{core} to a much lesser degree) centroid then deviates from the cloud centroid to a normalized distance of 0.27 (t=8 min). As cloud growth proceeds, B_{core} grows and its centroid coincides with the cloud's centroid. All cores' centroids are located near the cloud centroid during the majority of the growing and mature stages of the cloud, showing normalized distances <0.1. During dissipation (t>27 min), the cores' centroid locations start to distance away from the cloud's geometrical core followed by a reduction in distances due to the rapid loss of cloud volume. As mentioned above, it is shown that the regeneration of positive buoyancy at the end of cloud dissipation (t=40 min) takes place at the cloud edges, with normalized distance >0.5.

Finally, in Fig. 3d the fraction of pixels of each core contained within another core is shown. It can be seen that for the majority of cloud lifetime (up to t=33 min) B_{core} is subset (pixel fraction of 1) of RH_{core}, and the latter is a subset of W_{core}. As expected, the other three permutations of pixel fractions (e.g. W_{core} in B_{core}) show much lower values. The cloudy regions that are not included within B_{core} but are included within the two other cores are exclusively at the cloud's boundaries (see Fig. 2). The same pattern is seen for cloudy regions that are included within W_{core} but not in RH_{core}. During the dissipation stage of the cloud its self-containing property (i.e. $B_{core} \subseteq RH_{core} \subseteq W_{core}$) breaks down. Similar temporal evolutions as shown here are seen for the other simulated clouds (with various aerosol concentrations) in part II of this work.

5. Results - Cloud field simulations

5.1. Partition to different core types

To test the robustness of the observed behaviors seen for a single cloud~~ (and explained in the theoretical part)~~, it is necessary to check whether they also apply to large statistics of clouds in a cloud field. The BOMEX simulation is taken for the analyses here. We discard the first 3 hours of cloud field data, during which the field spins-up and its mean properties are unstable. In Fig. 4 the volume (f_{vol}) and mass (f_{mass}) fractions of the three core types are compared for all clouds (at all output times – every 1 min) in the CvM space. As seen in Fig. 1, the location of specific clouds in the CvM space indicates their stage in evolution. Most clouds are confined to the region between the adiabat and the inversion layer base except for small precipitating (lower left region) and dissipating clouds (upper left region). The color shades of the clouds indicate whether a cloud is mostly core (red), mostly margin (blue), or equally divided to core and margin (white).

As seen for the single cloud, the core mass fractions tend to be larger than core volume fractions, for all core types. This is due to the fact that LWC values in the cloud core regions are higher than in margin regions, so that a cloud might be core dominated in terms of mass while being margin dominated in terms of volume. Focusing on the differences between core types, the color patterns in the CvM space imply that B_{core} definition yields the lowest core fractions (for both mass and volume), followed by RH_{core} with higher values and W_{core} with the highest values. The absence of the B_{core} is especially noticeable for small clouds in their initial growth stages after formation (COG ~ 550 m and LWP < 1 g m^{-2}). Those same clouds show the highest core fractions for the other two core definitions. This large difference can be explained by the existence of the transition layer (as discussed in Sect. 3) near the lifting condensation level (LCL) in warm convective cloud fields which is the approximated height of a convective cloud base (Craven et al., 2002; Meerkötter and Bugliaro, 2009). Within this layer parcels rising from the sub-cloudy layer are generally colder than parcels subsiding from the cloudy layer. Thus, this transition layer clearly marks the lower edge of the buoyancy core as most convective clouds are initially negatively buoyant.

Generally, the growing cloud branch (i.e. the CvM region closest to the adiabat) shows the highest core fractions. The RH_{core} and W_{core} fractions decrease with cloud growth (increase in mass and COG height) while the B_{core} initially increases, shows the highest fraction values around the middle region of the growing branch and then decreases for the largest clouds. The transition from the growing branch to the dissipation branch is manifested by a transition from core dominated to margin dominated clouds (i.e. transition from red to blue shades). Mixed within the margin dominated dissipating cloud branch, a scatter of W_{core} dominated small clouds can be seen as well. These represent cloud fragments which shed off large clouds during their growing stages with positive vertical velocity. They are sometimes RH_{core} dominated as well but are strictly negatively buoyant. The few precipitating cloud fragments seen for this simulation (cloud scatter located below the adiabat) tend to be margin dominated, especially for the RH_{core}.

5.2. ~~Self-contained~~Subset properties of cores

From Fig. 4 it is clear that W_{core} tends to be the largest and B_{core} tends to be the smallest. To what degree however, are the cores ~~self-contained within~~subsets of one another as was seen for the single cloud simulation? It is also interesting to check whether the different physical cores are centered near the cloud's geometrical core. In

Fig. 5 the pixel fraction (f_{pixel}) of each core type within another core type is shown for all clouds in the CvM space. A f_{pixel}~~pixel fraction~~ of 1 (bright colors) indicates that the pixels of the specific core in question (labeled in each panel title) ~~completely~~ are a subset ~~overlap with the pixels~~ of the other core (also labeled in the panel title) and a f_{pixel}~~pixel fraction~~ of 0 (dark colors) indicates ~~zero overlap~~no intersection between the two cores in the cloud. It is seen that B_{core} tends to be a subset of both other cores, with f_{pixel}~~pixel fractions~~ around 0.75-1 for most of the growing branch area and large mass dissipating clouds which still have some positive buoyancy. The pixel fractions are higher for B_{core} inside W_{core} compared with B_{core} inside RH_{core}, but both show decrease with increase in growing branch cloud mass, meaning that chance for perfect self-containing of the cores decreases in large clouds.

The CvM space of RH_{core} inside W_{core} shows an even stronger relation between these two core types. For almost all growing branch clouds, the RH_{core} is a subset of W_{core} (i.e. $RH_{core} \subseteq W_{core}$). The decrease gradually with loss of cloud mass in the dissipation branch. The other three permutations of f_{pixel} (W_{core} inside B_{core}, W_{core} inside RH_{core}, and RH_{core} inside B_{core}) give an indication of cores sizes and of which cloud types show no overlap between different cores. As stated above, growing (dissipation) clouds show higher (lower) overlap between the different core types. The W_{core} is almost twice as large as the B_{core} and 30%-40% larger than the RH_{core} along most of the growing branch. In conclusion, we see a strong tendency for the ~~self-containing~~subset property of cores ($B_{core} \subseteq RH_{core} \subseteq W_{core}$) during the growth stages of clouds. This property ceases for dissipating and precipitating clouds, especially for the smaller clouds which show less overlap between core types.

In Fig. 6 the normalized distances (D_{norm}) between the total cloud centroid and each specific physical core centroid locations are evaluated. Along the growing branch the cloud centroid and physical cores' centroids tend to be of close proximity, while during cloud dissipation the cores' centroids tend to increase in distance from the cloud's center. This type of evolution is most prominent for the W_{core}, which shows a clear gradient of transition from small (dark colors) to large (bright colors) distances. The B_{core} shows a more complex transition, from intermediate distance values (~0.5) at cloud formation, to near zeros values along the mature part of the growing branch, back to large values in the dissipation branch. Along the growing branch RH_{core} shows distances comparable to the W_{core} (except for large distances at cloud formation). However, compared to the other two core types, RH_{core} shows the smallest distances to the geometrical core during cloud dissipation. This is manifested by a relative absence of bright colors for dissipating clouds in Fig. 6.

The prevalence of cloud edge B_{core} pixels during dissipation can be explained by adiabatic heating due to weak downdrafts (see Sect. 4.2, Part II) which are expected at the cloud periphery. The fact that there is little overlap between B_{core} and both W_{core} and RH_{core} pixels in dissipating clouds (see Fig. 5) serves to verify this assumption. The relative absence of isolated RH_{core} pixels at the cloud edges can be explained by the fact the pixels closest to the cloud's edge are most susceptible to mixing with non-cloudy air and evaporation, yielding subsaturation conditions. The innermost pixels are "protected" from such mixing and thus we can expect most RH_{core} pixels to be located near the geometrical core.

The W_{core} case is less intuitive. During cloud dissipation complex patterns of updrafts and downdrafts within the cloud can create scenarios where the W_{core} centroid is located anywhere in the cloud. However, the results show that most small dissipating clouds tend to have their W_{core} pixels concentrated at the cloud edges. Comparing Fig. 6 with Figs. 4 and 5, we can see that these pixels comprise only a tiny fraction of the already small clouds and do not overlap with RH_{core} and B_{core} pixels and thus are not related to significant convection processes. Further analysis shows that the maximum updrafts in these clouds rarely exceed 0.5 m/s (i.e. 90% of clouds with normalized distance > 0.9 have a maximum updraft of less than 0.5 m/s), and can thus be considered with near neutral vertical velocity.

5.3. Consistency of the cloud partition to core types

The results for cloud fields are summarized in Fig. 7 that presents the evolution of core fractions of continuous cloud entities (CCEs, see Sect. 2.5 for details) from formation to dissipation. Only CCEs that undergo a complete life cycle are averaged here. These CCEs fulfill the following four conditions: i) form near the LCL, ii) live for at least 10 minutes, ii) reach maximum cloud mean LWP values above 10 g m^{-2}, and iv) terminate with mass value below 10 g m^{-2}. As a test of generality, we performed this analysis for

Hawaiian and Amazonian warm cumulus cloud field simulations in addition to the BOMEX one. For each simulation, tens to hundreds of CCEs are collected (see panel titles) and their core fractions are averaged according to their normalized lifetimes (τ). Consistent results are seen for all three simulations. Clouds initiate with a W_{core} fraction of ~ 1, RH_{core} fraction of ~ 0.8, and B_{core} fraction of ~ 0.1. The former two core types' volume fraction decreases monotonically with lifetime, while the latter core type's volume fraction increases up to 0.3 at τ ~ 0.25, and then monotonically decreases for increasing τ. The fact that cloud's end their life cycle with non-zero volume fractions may indicate that some of the CCE terminate not because of full dissipation but rather because of significant splitting or merging events.

Normalized distances between core centroid and total cloud centroid (Fig. 7, middle column) tend to monotonically increase for RH_{core} and W_{core} with CCE lifetime for all simulations. The gradient of increase is larger at the later stages of CCE lifetime. Initially the W_{core} is closer to the geometrical core but at later stages of CCE lifetime (typically τ > 0.5) this switches and RH_{core} remains the closest. As seen above, for the first (second) half of CCE lifetime, the distance between B_{core} centroid and cloud centroid decreases (increases), starting at normalized distances above 0.4 for all simulations. The physical cores stay in proximity to the geometrical core for the majority of their lifetimes for the three cases. Taking the value 0.5 as a threshold for transition from centered physical cores to periphery physical cores, Bomex, Hawaii, and Amazon simulation CCEs' W_{core} cross this threshold at τ = 0.94, 0.9, and 0.86, respectively. Thus, the assumption that a cloud's core (by any definition) is also indicative of the cloud's centroid is true for the majority of a typical cloud's lifetime.

The analysis of self-containing core properties (Fig. 7, right column) shows that the assumption $B_{core} \subseteq RH_{core} \subseteq W_{core}$ is true for the initial formation stages of a cloud. Although the corresponding pixel fractions decrease slightly during the lifetime of the CCE, they remain above 0.9 (e.g. B_{core} is 90% contained within RH_{core}). A sharp decrease in pixel fractions is seen for τ > 0.8, as the overlaps between the different cores is reduced during dissipation stages of the cloud. For all simulations, the highest pixel fraction values are seen for the B_{core} inside W_{core} pair, followed by RH_{core} inside W_{core} pair, and B_{core} inside RH_{core} pair showing slightly lower values. In addition, it can be seen that the variance of average pixel fraction (per τ) increases with increase in τ. This is due to the fact the all CCEs initiate with almost identical characteristics but may terminate in very different ways. In part II of this work we show that this variance is highly influenced from precipitation which contributes to more significant interactions between clouds (Heiblum et al., 2016b). Indeed, the Amazon simulation shows the largest pixel fraction variance and produces the most precipitation out of the three simulations.

6. Summary

In this paper we study the partition of warm convective clouds to core and margin according to three different definitions: i) positive vertical velocity (W_{core}), ii) relative humidity supersaturation (RH_{core}), and iii) positive buoyancy (B_{core}), with emphasis on the differences between those definitions. Using theoretical considerations of both an adiabatic cloud column and a simple two parcel mixing model (see appendix A and B), we support our simulated results as we show that the B_{core} ~~must~~ is expected to be the smallest of the three. This finding is in line with previous works that showed that negative buoyancy is prevalent in cumulus clouds for a wide range of thermodynamic conditions (de Roode, 2008; Paluch, 1979; Taylor and Baker, 1991). This is due to the fact that entrainment into the core (i.e. mixing with non-cloudy environment or mixing with the margin regions of the cloud) ~~acts instantaneously to reduce cloud buoyancy values. In cases the mixed parcel is~~ may result in sub-saturation~~ed~~, followed by evaporation that~~occurs and~~ always has a negative net effect on buoyancy. The same process has an opposing effect on the relative humidity of the mixed parcel and acts to reach saturation. Entrainment (or mixing) also acts to decrease vertical velocity, but at slower manner compared to the time scales of changes in the buoyancy and relative humidity. In addition, the supersaturation equation (Eq. (3)) predicts that it is unlikely to ~~attain~~ maintain supersaturation in a cloudy volume with negative vertical velocity. Hence, W_{core} can be~~is~~ expected to be the largest of the three cores.

Using numerical simulations of both a single cloud and cloud fields of warm cumulus clouds, we show that during most stages of clouds' lifetime, W_{core} is indeed the largest of the three and B_{core} the smallest. In addition to the differences in their sizes, the three cores tend to be subsets of one another (and located around the cloud geometrical center), in the following order: $B_{core} \subseteq RH_{core} \subseteq W_{core}$. This property is most valid for a cloud at its initial stages and breaks down gradually during a cloud's lifetime. ~~The small B_{core} fractions (out of the total cloud) are due to two main reasons: i) buoyancy is strongly affected by mixing and evaporation, as the buoyant core is the first to disappear during the dissipation stages of a cloud, and ii) warm~~ The warm convective cloud fields simulated here typically have a transition layer near the lifting condensation level (LCL). ~~, where~~Thus, ~~ascending parcels are colder than descending parcels so~~ the lower parts of the clouds are negatively buoyant or even lack a B_{core} at formation. After cloud formation internal growth processes (i.e. condensation and latent heat release) increase the B_{core} until dissipation processes become dominant and the B_{core} ~~core~~ decreases quickly due to entrainment. In contrast, clouds are initially dominated by the W_{core} and RH_{core} (fractions close to 1). The fractions of these cores then decrease monotonically with cloud lifetime.

During dissipation stages, the clouds are mostly margin dominated, such that most of the small mass dissipation cloud fragments are entirely coreless. However, several small mass dissipating cloud fragments which shed off large cloud entities (with large COG height) may be core dominated, especially using the RH_{core} definition. The same is observed for small precipitating cloud fragments which reside below the convective cloud base. We note that the results here are similar for both volume and mass core fractions out the cloud's totals, with the core mass fractions being larger due to a skewed distribution of cloud LWC which favors the core regions. Moreover, we show that these results are consistent for various levels of aerosol concentrations (will be seen in Part II) and different thermodynamic profiles used to initialize the models.

With respect to cloud morphology, it is shown that during cloud growth, which comprises the majority of a warm cloud lifetime, the physical cores are centered near the cloud's geometrical core, as is intuitively expected from a cloud's core. This matches the convective cloud core-shell model. An exception to this is the initial growth stages, where the B_{core} centroid can be located far from the cloud's centroid. During dissipation, the core-shell model no longer applies to the clouds, as the cores decouple from the geometrical core and often comprise just a few isolated pixels at the cloud's edges. The W_{core} and B_{core} pixels tend to be more peripheral than RH_{core} during dissipation (see Sect. 5.2). Downdraft induced adiabatic heating at the clouds' edge (see more in Part II) promote positive buoyancy while decreasing the chance for supersaturation. During dissipation the overlap between different core types also decreases rapidly, implying that minor local effects enable core existence rather than cloud convection. Thus, only during mature growth stages can all three cores types can be considered interchangeable. In Part II of this work we use the insights gained here to understand aerosol effects on warm convective clouds, as are reflected by a cloud's partition to its core and margin.

Acknowledgements

The research leading to these results was supported by the Ministry of Science & Technology, Israel (grant no. 3-14444).

Appendix A: Buoyancy changes due to mixing of cloudy and non-cloudy parcels

Here we present a simple model for entrainment mixing between a cloudy parcel (either part of B_{core} or B_{margin}) and a dry environmental parcel. Entrainment mixes the momentum, heat, and humidity of the two parcels. We consider the mixing of a unit mass of cloud parcel which is defined by two criteria:

$$S_1 \geq 1$$
$$B_1 > 0 \; or \; B_1 < 0$$

with a unit mass of dry environment parcel, defined by:

$$S_2 < 1$$

and explore the properties of the resulting mixed parcel.

Assume that T_1, T_2, T_3 are the initial temperatures of the cloudy, environmental, and resulting mixed parcel, respectively. q_{v1}, q_{v2}, q_{v3}, $\theta_1, \theta_2, \theta_3$, and $q_{l_1}, q_{l_2}, q_{l_3}$ are their respective vapor mixing ratios, potential temperatures, and liquid water contents (LWC).

The change in buoyancy due to mixing will be:

$$dB_{mix} = g * \left(\frac{\theta_3 - \theta_1}{\theta_2} + 0.61(q_{v3} - q_{v1}) - (q_{l_3} - q_{l_1})\right) \quad \text{(A1)},$$

with

$$T_3 = \mu_1 \cdot T_1 + \mu_2 \cdot T_2 \quad \text{(A2)},$$

$$q_{v3} = \mu_1 \cdot q_{v1} + \mu_2 \cdot q_{v2} \quad \text{(A3)},$$

$$q_{l_3} = \mu_1 \cdot q_{l_1} + \mu_2 \cdot q_{l_2} \quad \text{(A4)},$$

where μ_1 and μ_2 are the corresponding mixing fractions. We assume that the mixed parcel is at the same height as the cloudy and environmental parcels, and that the mean environmental temperature at that height stays the same after mixing. The potential temperature (θ) is calculated using its definition.

After the mixing process, the resultant mixed parcel may be subsaturated ($S_3 < 1$), and cloud droplets start to evaporate. The evaporation process increases the humidity of the parcel. ((Korolev et al., 2016), Eq. (A8)) calculated the amount of the required liquid water for evaporation, in order to reach S=1 again:

$$\delta q = \frac{C_p R_v T_2^2}{L^2} ln\left(\frac{1+\frac{e_s(T_3)R_a L^2}{P C_p R_v^2 T_3^2}}{1+S_3\frac{e_s(T_3)R_a L^2}{P C_p R_v^2 T_3^2}}\right) \quad \text{(A5)},$$

Where C_p is a specific heat at constant pressure,$e_s(T_3)$ is the saturated vapor pressure for the mixed temperature, P is pressure, L is latent heat, R_v, R_a are individual gas constants for water vapor and dry air, respectively. If the mixed parcel contains sufficient LWC to evaporate δq amount of water, the mixed parcel will reach saturation. We note that Eq. (A5) holds for cases where $|T_1 - T_2| < 10^o C$, which is well within the range seen in our simulations of warm clouds.

Assuming the average environmental temperature stays the same after evaporation, the buoyancy after evaporation is calculated using the following formulas:

$$dB_{evap} = g \cdot \left(\frac{d\theta'_{evap}}{\theta_2} + 0.61 dq_{v_{evap}} - dq_{l_{evap}}\right) \quad \text{(A6)},$$

$$d\theta'_{evap} = dT_{evap} \quad \text{(A7)},$$

From the first law of thermodynamics:

$$C_p \cdot dT_{evap} = -L \cdot dq_{v_{evap}} \quad \text{(A8)}.$$

The water vapor is the amount of liquid water lost by evaporation:

$$dq_{v_{evap}} = -dq_{l_{evap}} = \delta q \quad \text{(A9)},$$

From the above we get:

$$dB_{evap} = g \cdot \delta q \left(1.61 - \frac{L}{C_p \theta_2}\right) \quad \text{(A10)}.$$

For a wide temperature range between $200 < \theta_2 < 300[K]$, dB_{evap} is always negative. This result is not trivial because evaporation both decreases the T and increases the q_v which have opposite effects. The total change in buoyancy is taken as the sum of dB_{evap} and dB_{mix}.

Figure A1 presents a phase space of possible changes in cloudy pixel buoyancy due to mixing with outside air, for various thermodynamic conditions, and a mixing fraction of 0.5. The initial cloudy parcel is chosen to be saturated (S=1) and includes a LWC of 1 g kg^{-1}. The pressure is assumed to be 850 mb, and the temperature 15^{o}C. However, we note that the conclusions here apply to all atmospherically relevant values of pressure, temperature, supersaturation (values of RH>100%), and LWC in warm clouds. The X-axis in Fig. A1 spans a range of non-cloudy environment relative humidity values (60% < RH < 100%), and the Y-axis spans a temperature difference range between the cloud and the environment parcels ($-3° < dT < 3°$). The initial (B_i) and final (B_f, after entrainment) buoyancy values, and the differences between them can be either positive or negative. The regions of B_i>0 (B_i<0) in fact illustrate the effects of entrainment on B_{core} (B_{margin}) parcels.

Appendix B: **Buoyancy changes due to mixing of core and margin parcels**

Following the notations of appendix A, we now consider the mixing of two cloudy parcels, one part of B_{core} and one part ofB_{margin}. For simplicity, we choose the case where both parcels are saturated and have the same LWC of 0.5 g kg^{-1}:

$$\begin{gathered} S_{core} = S_{margin} = S_{cloud} = 1 \\ q_{l_{core}} = q_{l_{margin}} = q_{l_{cloud}} = 0.5 \end{gathered} \quad \text{(B1)}.$$

The buoyancy of each cloudy parcel is determined in reference to the environmental temperature and humidity, $T_{env}, q_{v_{env}}$, so that:

$$B_{cloud} = g * \left(\frac{\theta_{cloud} - \theta_{env}}{\theta_{env}} + 0.61\left(q_{v_{cloud}} - q_{v_{env}}\right) - q_{l_{cloud}}\right) \qquad \text{(B2).}$$

As mentioned in the main text, we take a temperature range of $T_{env} - 3°c < T_{cloud} < T_{env} + 3°c$. Each cloudy parcel's temperature also dictates its saturation vapor pressure $e_s(T_{cloud})$ and therefore also its humidity content, $q_{v_{cloud}}$. Plugging these into Eq. (B2), one can associate each temperature/humidity pair with the B_{core} or B_{margin}:

$$\begin{gathered} T_{core} = T_{cloud}(B_{cloud} > 0),\ q_{v_{core}} = q_{v_{cloud}}(B_{cloud} > 0) \\ T_{margin} = T_{cloud}(B_{cloud} < 0), q_{v_{margin}} = q_{v_{cloud}}(B_{cloud} < 0) \end{gathered} \qquad \text{(B3).}$$

The core and margin parcels can then be mixed (see appendix A) yielding a mixed parcel temperature and humidity content, and thus a new relative humidity. The buoyancy of the mixed parcel is obtained by inserting these parameters in Eq. (B2).

In Fig. B1 the resultant buoyancy values and RH values after the mixing of B_{core} parcels with B_{margin} parcels are shown. As defined in Appendix A, temperature differences between the parcels and the environment are confined to ±3^{o}C. The reference environmental temperature, pressure, and RH are taken to be 15^{o}C, 850 mb, and 90%, respectively. We note the main differences between this section and Appendix A are the absence of evaporation and the fact that the core and margin thermodynamic variables are the ones that vary while the reference environmental ones are kept constant.

It can be seen that all negatively buoyant parcels are colder than the environment and nearly all positively buoyant parcels are warmer than the environment, except for a small fraction that are slightly colder but positively buoyant due to the increased humidity. The transition from $B_f>0$ to $B_f<0$ near the 1 to 1 line indicates that B_f is approximately linearly dependent on the temperature differences with respect to the environment. In other words, if $|T_{core} - T_{env}| > |T_{margin} - T_{env}|$, the mixed parcel is expected to be part of the B_{core} (i.e. $B_f>0$). The exponential increase in saturation vapor pressure with temperature is demonstrated by the results of the mixed parcel final RH, which all show supersaturation values. Additional sensitivity tests were performed for this analysis, showing only weak dependencies on environmental parameter values, while maintaining the main conclusions.

Figures

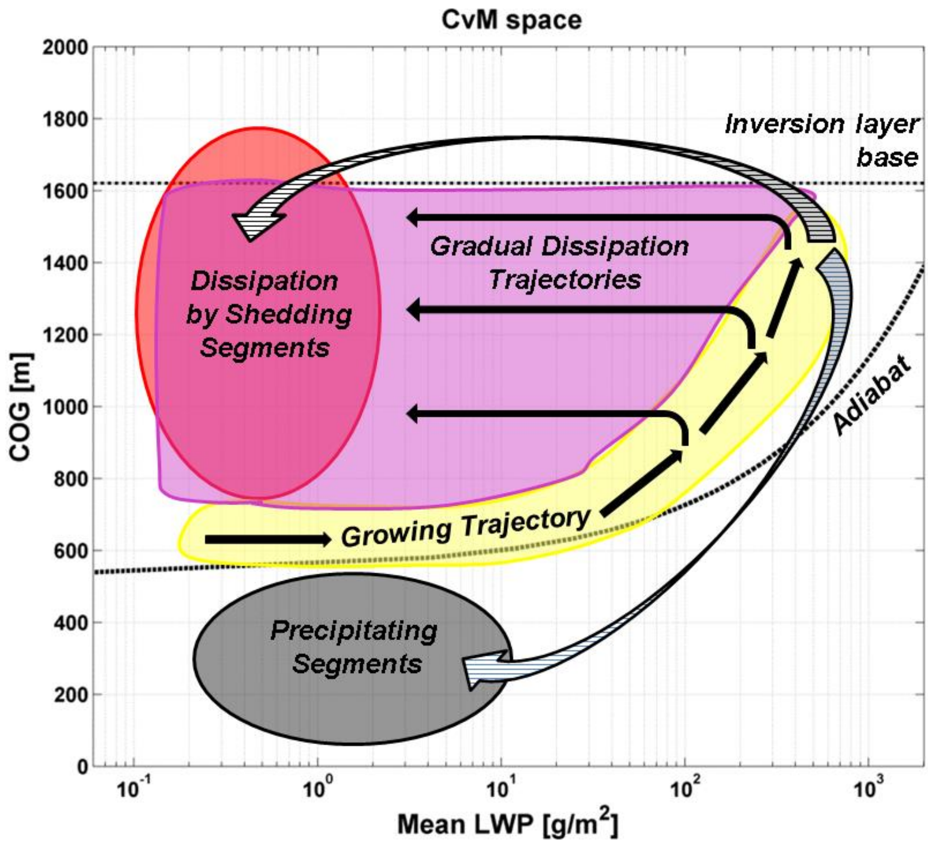

Figure 1. A schematic representation of a cloud field Center-of-gravity height (Y-Axis) vs. Mass (X-Axis) phase space (CvM in short). The majority of clouds are confined to the region between the adiabatic approximation (curved dashed line) and the inversion layer base height (horizontal dashed line). The yellow, magenta, red, and grey shaded regions represent cloud growth, gradual dissipation, cloud fragments which shed off large clouds, and cloud fragments which shed off precipitating clouds, respectively. The black arrows represent continuous trajectories of cloud growth and dissipation. The hatched arrows represent two possible discontinuous trajectories of cloud dissipation where clouds shed segments.

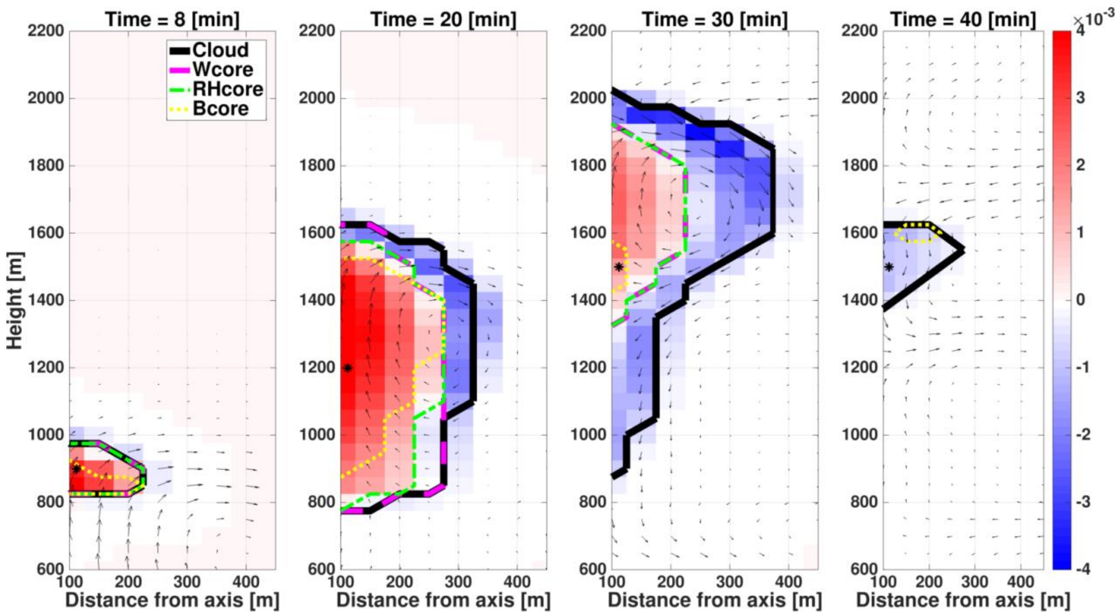

Figure 2. Four vertical cross-sections (at t=8, 20, 30, 40 minutes) during the single cloud simulation. Y-axis represents height [m] and X-axis represents the distance from the axis [m]. The black, magenta, green and yellow lines represent the cloud, W_{core}, RH_{core} and B_{core}, respectively. The black arrows represent the wind, the background represents the condensation (red) and evaporation rate (blue) [g kg^{-1} s^{-1}], and the black asterisks indicate the vertical location of the cloud centroid. Note that in some cases the lines indicating core boundaries overlap (mainly seen for RH and W cores).

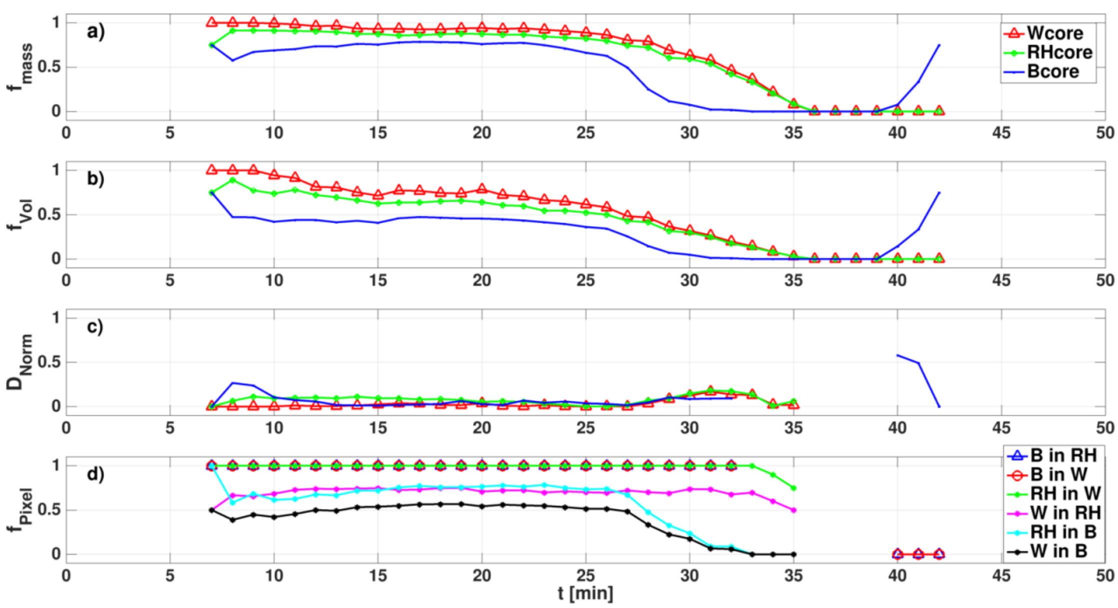

Figure 3. Temporal evolution of selected core properties, including: (a) The fraction of the cores' mass from the total cloud mass (f_{mass}), (b) the fraction of the cores' volume from the total cloud volume (f_{vol}), (c) the normalized distance between cloud centroid and core centroid (D_{norm}), and (d) the fraction of cores' pixels contained within another core (f_{pixel}), including all six permutations. See panel legends for descriptions of line colors.

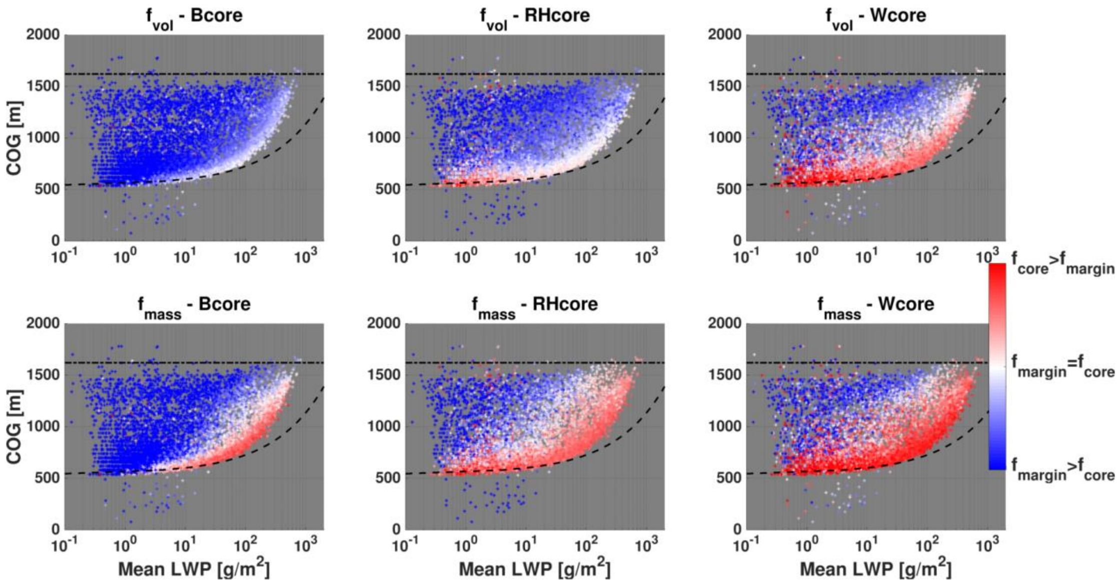

Figure 4. CvM phase space diagrams of B_{core} (left column), RH_{core} (middle column), and W_{core} (right column) fractions for all clouds between 3 h and 8 h in the BOMEX simulation. Both volume fractions (f_{vol}, upper panels) and mass fractions (f_{mass} lower panels) are shown. The red (blue) colors indicate a core fraction above (below) 0.5. For a general description of CvM space characteristics the reader is referred to Sect. 2.4.

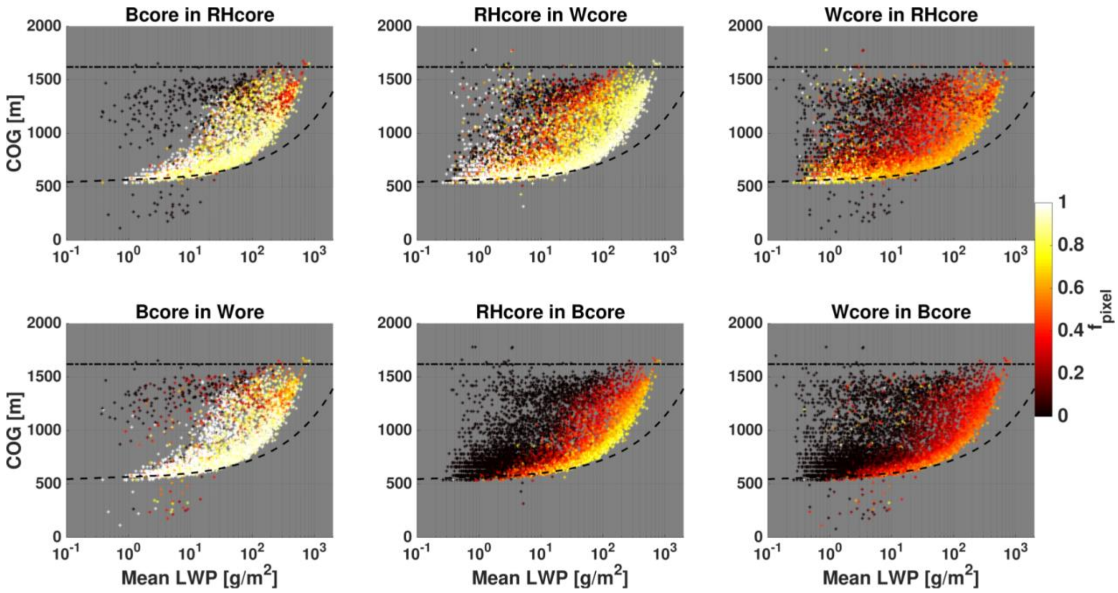

Figure 5. CvM phase space diagrams of pixel fractions (f_{pixel}) of each of the three cores within another core, including six different permutations (as indicated in the panel titles). Bright colors indicate high pixel fractions (large overlap between two core types) while dark colors indicate low pixel fraction (little overlap between two core types). The differences in the scatter density and location for different panels are due to the fact that only clouds which contain a core fraction above zero (for the core in question) are considered. For example, for the Buoy in RH panel (upper left), only cloud that contain some pixels with positive buoyancy are considered.

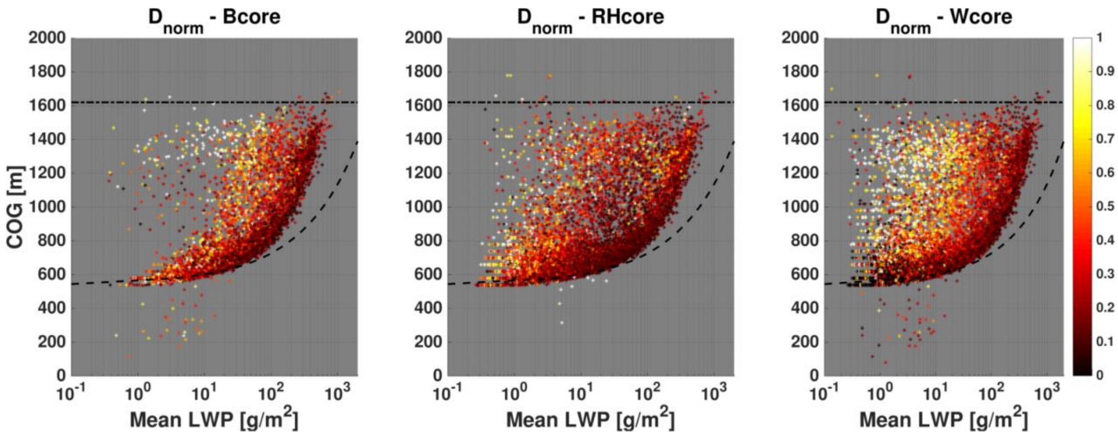

Figure 6. CvM phase space diagrams of distances between core centroid location and cloud centroid location, for the three different physical core types. The distances are normalized by the cloud volume radius (approximately the largest distance possible).

Bright (dark) colors indicates large (small) distances. As seen in Fig. 5, only clouds which contain a core fraction above zero (for the core in question) are considered.

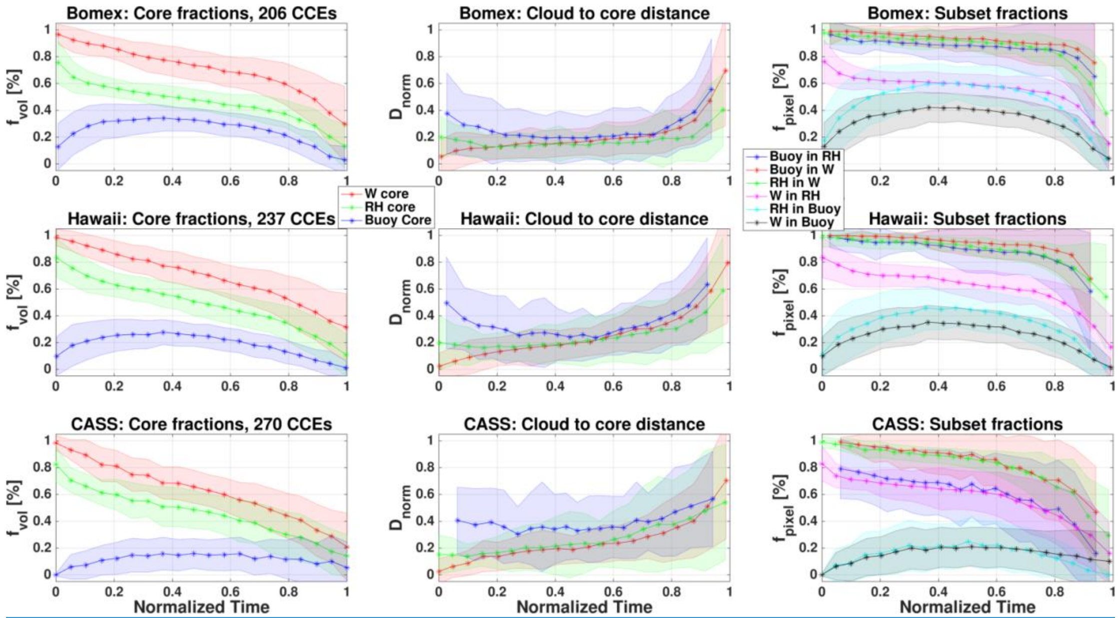

Figure 7. Normalized time (τ) series of CCE averaged core fractions for the BOMEX (upper row), Hawaii (middle row), and Amazon (bottom row) simulations. Both core volume fractions (left column), normalized distances between cloud and core centroid locations (middle column), and pixel fractions of one core within another (right column) are considered. Line colors indicated different core types (see legends), while corresponding shaded color regions indicate the standard deviation. Normalized time enables to average together CCEs with different lifetimes, from formation to dissipation. The number of CCEs averaged together for each simulation is included in the left column panel titles.

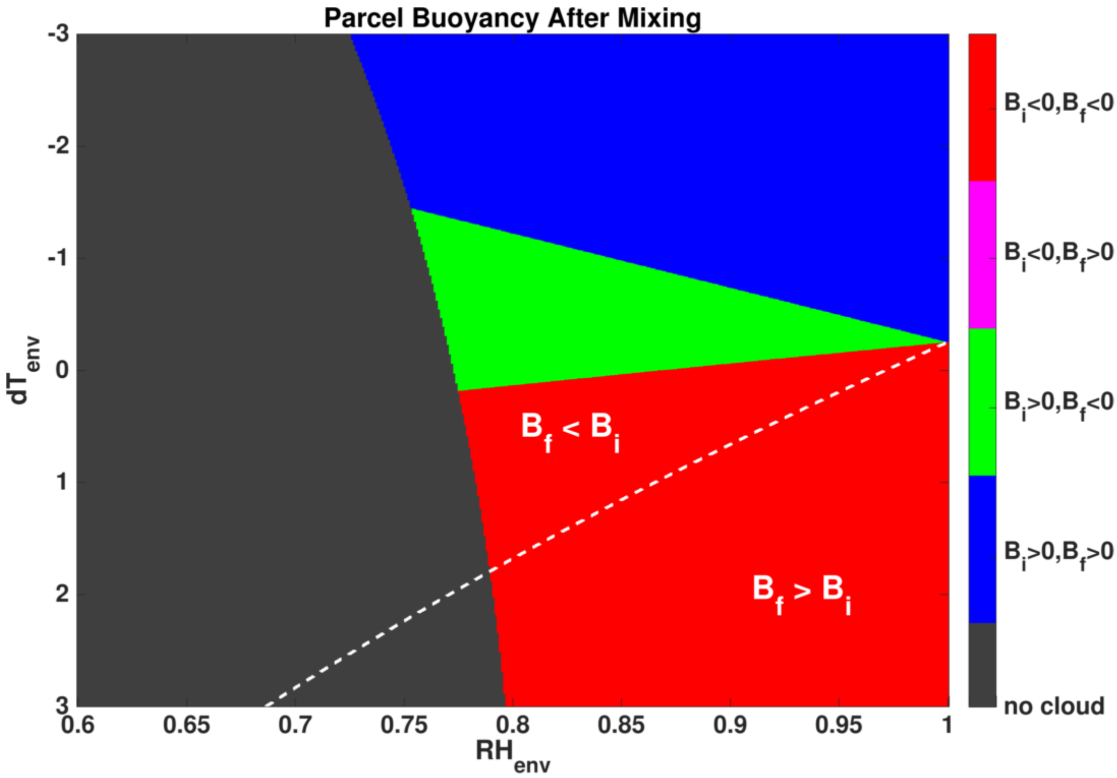

Figure A1. Phase space presenting the effects of entrainment on cloud buoyancy, where the initial cloudy parcel buoyancy (Bi) and final mixed parcel buoyancy (Bf) are considered. A mixing fraction of 0.5 is chosen. The initial cloudy parcel is saturated (S=1), has a temperature of 15°C, pressure of 850 mb, and LWC of 1 g kg^{-1}*. The X-axis spans a range of environment relative humidity values (*RH_{env}*), and the Y-axis a temperature difference (*$dT_{env}=T_{env}-T_{cld}$*) range between the cloud and the environment parcels. Red color represents *$B_i<0$ & $B_f<0$ *(i.e. parcel stays negatively buoyant after the mixing), magenta represents *$B_i<0$ & $B_f>0$ *(i.e. transition from negative to positive buoyancy), green represents *$B_i>0$ & $B_f<0$ *(i.e. transition from positive to negative buoyancy), and blue represents *$B_i>0$ & $B_f>0$ *(i.e. parcel stays positively buoyant). The grey color represents mixed parcels that were depleted from water (LWC value lower than 0.01 g kg*$^{-1}$*) after evaporation, and are considered non-cloudy. The white line separates between areas where *$B_f>B_i$ *and* $B_f<B_i$.

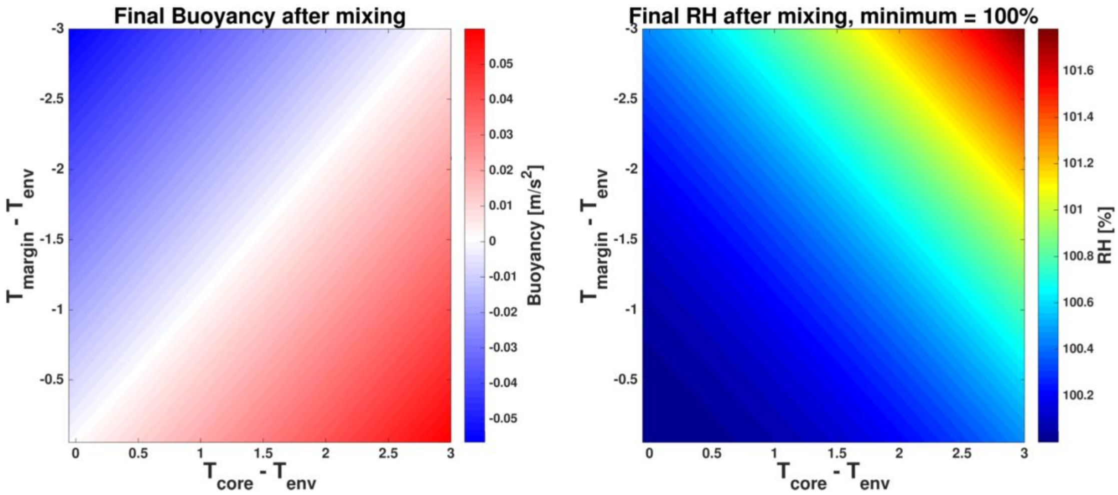

Figure B1. Phase space presenting the resultant buoyancy (left panel) and relative humidity (RH, right panel) when mixing B_{core} and B_{margin} parcels with equal RH but different temperatures. A mixing fraction of 0.5 is chosen. Both parcels are initially saturated (RH=100%), and have a LWC of 0.5 g kg^{-1}. The environment has a temperature of $15^{o}C$ and pressure of 850 mb. The X(Y)-axis spans the range of temperature differences between the B_{core} (B_{margin}) parcel and the environment.

References

Ackerman, B.: Buoyancy and precipitation in tropical cumuli, J. Meteor., 13(3), 302–310, doi:10.1175/1520-0469(1956)013<0302:BAPITC>2.0.CO;2, 1956.

Altaratz, O., Koren, I., Reisin, T., Kostinski, A., Feingold, G., Levin, Z. and Yin, Y.: Aerosols' influence on the interplay between condensation, evaporation and rain in warm cumulus cloud, Atmos. Chem. Phys., 8(1), 15–24, doi:10.5194/acp-8-15-2008, 2008.

Betts, A. K.: Non-precipitating cumulus convection and its parameterization, Q.J Royal Met. Soc., 99(419), 178–196, doi:10.1002/qj.49709941915, 1973.

Burnet, F. and Brenguier, J.-L.: The onset of precipitation in warm cumulus clouds: An observational case-study, Q.J Royal Met. Soc., doi:10.1002/qj.552, 2010.

Craven, J. P., Jewell, R. E. and Brooks, H. E.: Comparison between Observed Convective Cloud-Base Heights and Lifting Condensation Level for Two Different Lifted Parcels, Wea. Forecasting, 17(4), 885–890, doi:10.1175/1520-0434(2002)017<0885:CBOCCB>2.0.CO;2, 2002.

Dagan, G., Koren, I. and Altaratz, O.: Competition between core and periphery-based processes in warm convective clouds – from invigoration to suppression, Atmos. Chem. Phys., 15(5), 2749–2760, doi:10.5194/acp-15-2749-2015, 2015.

Dawe, J. T. and Austin, P. H.: Statistical analysis of an LES shallow cumulus cloud ensemble using a' ' cloud tracking algorithm, Atmos. Chem. Phys., 12(2), 1101–1119, doi:10.5194/acp-12-1101-2012, 2012.

de Roode, S. R.: Thermodynamics of cumulus clouds, Física de la Tierra; Vol 19 (2007), 2008.

de Roode, S. R. and Bretherton, C. S.: Mass-Flux Budgets of Shallow Cumulus Clouds, J. Atmos. Sci., 60(1), 137–151, doi:10.1175/1520-0469(2003)060<0137:MFBOSC>2.0.CO;2, 2003.

de Roode, S. R., Siebesma, A. P., Jonker, H. J. J. and de Voogd, Y.: Parameterization of the vertical velocity equation for shallow cumulus clouds, Mon. Wea. Rev., 140(8), 2424–2436, doi:10.1175/MWR-D-11-00277.1, 2012.

de Rooy, W. C. and Siebesma, A. P.: A simple parameterization for detrainment in shallow cumulus, Mon. Wea. Rev., 136(2), 560–576, doi:10.1175/2007MWR2201.1, 2008.

Derbyshire, S. H., Maidens, A. V., Milton, S. F., Stratton, R. A. and Willett, M. R.: Adaptive detrainment in a convective parametrization, Q.J Royal Met. Soc., 137(660), 1856–1871, doi:10.1002/qj.875, 2011.

Dias, M. A., Dias, P. L. S., Longo, M., Fitzjarrald, D. R. and Denning, A. S.: LBA-ECO CD-01 Meteorological Data, Tapajos and Amazon Rivers, Santarem, Brazil: 2001, Data set.,, 2012.

Emanuel, K. A.: A Scheme for Representing Cumulus Convection in Large-Scale Models, J. Atmos. Sci., 48(21), 2313–2329, doi:10.1175/1520-0469(1991)048<2313:ASFRCC>2.0.CO;2, 1991.

Feingold, G., Levin, Z. and Tzivion (Tzitzvashvili), S.: The evolution of raindrop spectra. part III: downdraft generation in an axisymmetrical rainshaft model, J. Atmos. Sci., 48(2), 315–330, doi:10.1175/1520-0469(1991)048<0315:TEORSP>2.0.CO;2, 1991.

Feingold, G., Tzivion (Tzitzvashvili), S. and Leviv, Z.: Evolution of raindrop spectra. part I: solution to the stochastic collection/breakup equation using the method of moments, J. Atmos. Sci., 45(22), 3387–3399, doi:10.1175/1520-0469(1988)045<3387:EORSPI>2.0.CO;2, 1988.

Garstang, M. and Betts, A. K.: A review of the tropical boundary layer and cumulus convection: structure, parameterization, and modeling, Bull. Amer. Meteor. Soc., 55(10), 1195–1205, doi:10.1175/1520-0477(1974)055<1195:AROTTB>2.0.CO;2, 1974.

Grabowski, W. W. and Jarecka, D.: Modeling condensation in shallow nonprecipitating convection, J. Atmos. Sci., 72(12), 4661–4679, doi:10.1175/JAS-D-15-0091.1, 2015.

Grant, A. L. M. and Lock, A. P.: The turbulent kinetic energy budget for shallow cumulus convection, Q.J Royal Met. Soc., 130(597), 401–422, doi:10.1256/qj.03.50, 2004.

Gregory, D. and Rowntree, P. R.: A Mass Flux Convection Scheme with Representation of Cloud Ensemble Characteristics and Stability-Dependent Closure, Mon. Wea. Rev., 118(7), 1483–1506, doi:10.1175/1520-0493(1990)118<1483:AMFCSW>2.0.CO;2, 1990.

Heiblum, R. H., Altaratz, O., Koren, I., Feingold, G., Kostinski, A. B., Khain, A. P., Ovchinnikov, M., Fredj, E., Dagan, G., Pinto, L., Yaish, R. and Chen, Q.: Characterization of cumulus cloud fields using trajectories in the center of gravity versus water mass phase space: 1. Cloud tracking and phase space description, J. Geophys. Res. Atmos., 121(11), 6336–6355, doi:10.1002/2015JD024186, 2016a.

Heiblum, R. H., Altaratz, O., Koren, I., Feingold, G., Kostinski, A. B., Khain, A. P., Ovchinnikov, M., Fredj, E., Dagan, G., Pinto, L., Yaish, R. and Chen, Q.: Characterization of cumulus cloud fields using trajectories in the center of gravity versus water mass phase space: 2. Aerosol effects on warm convective clouds, J. Geophys. Res. Atmos., 121(11), 6356–6373, doi:10.1002/2015JD024193, 2016b.

Hernandez-Deckers, D. and Sherwood, S. C.: A numerical investigation of cumulus thermals, J. Atmos. Sci., 73(10), 4117–4136, doi:10.1175/JAS-D-15-0385.1, 2016.

Heus, T., J. Pols, C. F., J. Jonker, H. J., A. Van den Akker, H. E. and H. Lenschow, D.: Observational validation of the compensating mass flux through the shell around cumulus clouds, Q.J Royal Met. Soc., 135(638), 101–112, doi:10.1002/qj.358, 2009a.

Heus, T. and Jonker, H. J. J.: Subsiding Shells around Shallow Cumulus Clouds, J. Atmos. Sci., 65(3), 1003–1018, doi:10.1175/2007JAS2322.1, 2008.

Heus, T., Jonker, H. J. J., Van den Akker, H. E. A., Griffith, E. J., Koutek, M. and Post, F. H.: A statistical approach to the life cycle analysis of cumulus clouds selected in a virtual reality environment, J. Geophys. Res., 114(D6), doi:10.1029/2008JD010917, 2009b.

Heus, T. and Seifert, A.: Automated tracking of shallow cumulus clouds in large domain, long duration large eddy simulations, Geosci. Model Dev., 6(4), 1261–1273, doi:10.5194/gmd-6-1261-2013, 2013.

Holland, J. Z. and Rasmusson, E. M.: Measurements of the Atmospheric Mass, Energy, and Momentum Budgets Over a 500-Kilometer Square of Tropical Ocean, Mon. Wea. Rev., 101(1), 44–55, doi:10.1175/1520-0493(1973)101<0044:MOTAME>2.3.CO;2, 1973.

IPCC: Climate Change 2013: The Physical Science Basis. Working Group I Contribution to the Fifth Assessment Report of the IPCC, Cambridge Univ. Press, New York., 2013.

Jaenicke, R.: 9.3.1 Physical properties, in Physical and chemical properties of the air, edited by G. Fischer, pp. 405–420, Springer-Verlag, Berlin/Heidelberg., 1988.

Jiang, H. and Feingold, G.: Effect of aerosol on warm convective clouds: Aerosol-cloud-surface flux feedbacks in a new coupled large eddy model, J. Geophys. Res., 111(D1), doi:10.1029/2005JD006138, 2006.

Jonker, H. J. J., Heus, T. and Sullivan, P. P.: A refined view of vertical mass transport by cumulus convection, Geophys. Res. Lett., 35(7), doi:10.1029/2007GL032606, 2008.

Kain, J. S. and Fritsch, J. M.: A One-Dimensional Entraining/Detraining Plume Model and Its Application in Convective Parameterization, J. Atmos. Sci., 47(23), 2784–2802, doi:10.1175/1520-0469(1990)047<2784:AODEPM>2.0.CO;2, 1990.

Khain, A. P., Beheng, K. D., Heymsfield, A., Korolev, A., Krichak, S. O., Levin, Z., Pinsky, M., Phillips, V., Prabhakaran, T., Teller, A., van den Heever, S. C. and Yano, J. I.: Representation of microphysical processes in cloud-resolving models: Spectral (bin) microphysics versus bulk parameterization, Rev. Geophys., 53(2), 247–322, doi:10.1002/2014RG000468, 2015.

Khain, A., Pokrovsky, A., Pinsky, M., Seifert, A. and Phillips, V.: Simulation of Effects of Atmospheric Aerosols on Deep Turbulent Convective Clouds Using a Spectral Microphysics Mixed-Phase Cumulus Cloud Model. Part I: Model Description and Possible Applications, J. Atmos. Sci., 61(24), 2963–2982, doi:10.1175/JAS-3350.1, 2004.

Khairoutdinov, M. F., Krueger, S. K., Moeng, C.-H., Bogenschutz, P. A. and Randall, D. A.: Large-eddy simulation of maritime deep tropical convection, J. Adv. Model. Earth Syst., 2, 15, doi:10.3894/JAMES.2009.1.15, 2009.

Khairoutdinov, M. F. and Randall, D. A.: Cloud resolving modeling of the ARM summer 1997 IOP: model formulation, results, uncertainties, and sensitivities, J. Atmos. Sci., 60(4), 607–625, doi:10.1175/1520-0469(2003)060<0607:CRMOTA>2.0.CO;2, 2003.

Korolev, A., Khain, A., Pinsky, M. and French, J.: Theoretical study of mixing in liquid clouds – Part 1: Classical concepts, Atmos. Chem. Phys., 16(14), 9235–9254, doi:10.5194/acp-16-9235-2016, 2016.

Kumar, V. V., Jakob, C., Protat, A., Williams, C. R. and May, P. T.: Mass-Flux Characteristics of Tropical Cumulus Clouds from Wind Profiler Observations at Darwin, Australia, J. Atmos. Sci., 72(5), 1837–1855, doi:10.1175/JAS-D-14-0259.1, 2015.

Lebo, Z. J. and Seinfeld, J. H.: Theoretical basis for convective invigoration due to increased aerosol concentration, Atmos. Chem. Phys., 11(11), 5407–5429, doi:10.5194/acp-11-5407-2011, 2011.

Lehmann, K., Siebert, H. and Shaw, R. A.: Homogeneous and inhomogeneous mixing in cumulus clouds: Dependence on local turbulence structure, Journal of the Atmospheric Sciences, 66(12), 3641–3659, 2009.

Malkus, J. S.: On the structure of the trade wind moist layer, Woods Hole Oceanographic Institution, Woods Hole, MA., 1957.

Meerkötter, R. and Bugliaro, L.: Diurnal evolution of cloud base heights in convective cloud fields from MSG/SEVIRI data, Atmos. Chem. Phys., 9(5), 1767–1778, doi:10.5194/acp-9-1767-2009, 2009.

Morrison, H.: On the robustness of aerosol effects on an idealized supercell storm simulated with a cloud system-resolving model, Atmos. Chem. Phys., 12(16), 7689–7705, doi:10.5194/acp-12-7689-2012, 2012.

Morrison, H.: Impacts of updraft size and dimensionality on the perturbation pressure and vertical velocity in cumulus convection. part I: simple, generalized analytic solutions, J. Atmos. Sci., 73(4), 1441–1454, doi:10.1175/JAS-D-15-0040.1, 2016a.

Morrison, H.: Impacts of updraft size and dimensionality on the perturbation pressure and vertical velocity in cumulus convection. part II: comparison of theoretical and numerical solutions and fully dynamical simulations, J. Atmos. Sci., 73(4), 1455–1480, doi:10.1175/JAS-D-15-0041.1, 2016b.

Morrison, H.: An analytic description of the structure and evolution of growing deep cumulus updrafts, J. Atmos. Sci., 74(3), 809–834, doi:10.1175/JAS-D-16-0234.1, 2017.

Neggers, R. A. J., Stevens, B. and Neelin, J. D.: Variance scaling in shallow-cumulus-topped mixed layers, Q.J Royal Met. Soc., 133(628), 1629–1641, doi:10.1002/qj.105, 2007.

Paluch, I. R.: The entrainment mechanism in colorado cumuli, J. Atmos. Sci., 36(12), 2467–2478, doi:10.1175/1520-0469(1979)036<2467:TEMICC>2.0.CO;2, 1979.

Peters, J. M.: The Impact of Effective Buoyancy and Dynamic Pressure Forcing on Vertical Velocities within Two-Dimensional Updrafts, J. Atmos. Sci., 73(11), 4531–4551, doi:10.1175/JAS-D-16-0016.1, 2016.

Pinsky, M., Mazin, I. P., Korolev, A. and Khain, A.: Supersaturation and diffusional droplet growth in liquid clouds, J. Atmos. Sci., 70(9), 2778–2793, doi:10.1175/JAS-D-12-077.1, 2013.

Reisin, T., Levin, Z. and Tzivion, S.: Rain Production in Convective Clouds As Simulated in an Axisymmetric Model with Detailed Microphysics. Part I: Description of the Model, J. Atmos. Sci., 53(3), 497–519, doi:10.1175/1520-0469(1996)053<0497:RPICCA>2.0.CO;2, 1996.

Rennó, N. O. and Ingersoll, A. P.: Natural convection as a heat engine: A theory for CAPE, J. Atmos. Sci., 53(4), 572–585, doi:10.1175/1520-0469(1996)053<0572:NCAAHE>2.0.CO;2, 1996.

Reutter, P., Su, H., Trentmann, J., Simmel, M., Rose, D., Gunthe, S. S., Wernli, H., Andreae, M. O. and Pöschl, U.: Aerosol- and updraft-limited regimes of cloud droplet formation: influence of particle number, size and hygroscopicity on the activation of cloud condensation nuclei (CCN), Atmos. Chem. Phys., 9(18), 7067–7080, doi:10.5194/acp-9-7067-2009, 2009.

Rodts, S. M. A., Duynkerke, P. G. and Jonker, H. J. J.: Size Distributions and Dynamical Properties of Shallow Cumulus Clouds from Aircraft Observations and Satellite Data, J. Atmos. Sci., 60(16), 1895–1912, doi:10.1175/1520-0469(2003)060<1895:SDADPO>2.0.CO;2, 2003.

Rogers, R. R. and Yau, M. K.: A Short Course in Cloud Physics, International Series in Natural Philosophy,, 1989.

Romps, D. M. and Charn, A. B.: Sticky Thermals: Evidence for a Dominant Balance between Buoyancy and Drag in Cloud Updrafts, J. Atmos. Sci., 72(8), 2890–2901, doi:10.1175/JAS-D-15-0042.1, 2015.

Seigel, R. B.: Shallow Cumulus Mixing and Subcloud-Layer Responses to Variations in Aerosol Loading, J. Atmos. Sci., 71(7), 2581–2603, doi:10.1175/JAS-D-13-0352.1, 2014.

Seiki, T. and Nakajima, T.: Aerosol effects of the condensation process on a convective cloud simulation, J. Atmos. Sci., 71(2), 833–853, doi:10.1175/JAS-D-12-0195.1, 2014.

Siebesma, A. P., Bretherton, C. S., Brown, A., Chlond, A., Cuxart, J., Duynkerke, P. G., Jiang, H., Khairoutdinov, M., Lewellen, D., Moeng, C.-H., Sanchez, E., Stevens, B. and Stevens, D. E.: A large eddy simulation intercomparison study of shallow cumulus convection, J. Atmos. Sci., 60(10), 1201–1219, doi:10.1175/1520-0469(2003)60<1201:ALESIS>2.0.CO;2, 2003.

Siebesma, A. P. and Cuijpers, J. W. M.: Evaluation of parametric assumptions for shallow cumulus convection, J. Atmos. Sci., 52(6), 650–666, doi:10.1175/1520-0469(1995)052<0650:EOPAFS>2.0.CO;2, 1995.

Sinkevich, A. A. and Lawson, R. P.: A survey of temperature measurements in convective clouds, J. Appl. Meteor., 44(7), 1133–1145, doi:10.1175/JAM2247.1, 2005.

Taylor, G. R. and Baker, M. B.: Entrainment and detrainment in cumulus clouds, J. Atmos. Sci., 48(1), 112–121, doi:10.1175/1520-0469(1991)048<0112:EADICC>2.0.CO;2, 1991.

Trenberth, K. E., Fasullo, J. T. and Kiehl, J.: Earth’s global energy budget, Bull. Amer. Meteor. Soc., 90(3), 311–323, doi:10.1175/2008BAMS2634.1, 2009.

Tzivion (Tzitzvashvili), S., Feingold, G. and Levin, Z.: The evolution of raindrop spectra. part II: collisional collection/breakup and evaporation in a rainshaft, J. Atmos. Sci., 46(21), 3312–3328, doi:10.1175/1520-0469(1989)046<3312:TEORSP>2.0.CO;2, 1989.

Tzivion, S., Reisin, T. and Levin, Z.: Numerical simulation of hygroscopic seeding in a convective cloud, J. Appl. Meteor., 33(2), 252–267, doi:10.1175/1520-0450(1994)033<0252:NSOHSI>2.0.CO;2, 1994.

Wang, Y., Geerts, B. and French, J.: Dynamics of the cumulus cloud margin: an observational study, J. Atmos. Sci., 66(12), 3660–3677, doi:10.1175/2009JAS3129.1, 2009.

Wei, D., Blyth, A. M. and Raymond, D. J.: Buoyancy of convective clouds in TOGA COARE, Journal of the atmospheric sciences, 55(22), 3381–3391, 1998.

Williams, E. and Stanfill, S.: The physical origin of the land–ocean contrast in lightning activity, Comptes Rendus Physique, 3(10), 1277–1292, doi:10.1016/S1631-0705(02)01407-X, 2002.

Xue, H. and Feingold, G.: Large-Eddy Simulations of Trade Wind Cumuli: Investigation of Aerosol Indirect Effects, J. Atmos. Sci., 63(6), 1605–1622, doi:10.1175/JAS3706.1, 2006.

Yano, J.-I., Chaboureau, J.-P. and Guichard, F.: A generalization of CAPE into potential-energy convertibility, Q.J Royal Met. Soc., 131(607), 861–875, doi:10.1256/qj.03.188, 2005.